Chapter 3

EXPLORATORY EXPERIMENTS

In the previous chapter the nature of ice rubble shear strength was explored. It was found that rubble behaviour is state-dependent and non-unique with very little full-scale data from the field for guidance. It was then shown that few laboratory programs have been undertaken specifically to model structures interacting with unconsolidated ridge keels. Keel load models in the literature were reviewed and a sensitivity study demonstrated that significant variation exists in model flexibility and output. Thus it has been shown that considerable parametric and model uncertainties exist, that the two are correlated and that this problem, at least in part, arises from a scarcity of field and laboratory data.

In this chapter a succession of exploratory experimental programs are described in which the purpose was to establish a database for ridge keel model development and calibration. The first, a broad study using simple techniques, looked at many ice rubble properties and keel-structure interaction scenarios. This program was followed by larger-scale sophisticated interaction experiments, sponsored by government and industry, and carried out at IMD by a research team. As in the first experimental program the failure mechanisms of unconsolidated ridges were observed and associated interaction forces were recorded. The last laboratory program described in this Chapter is one in which an *in situ* direct shear technique was developed for measuring ridge keel shear strength.

Data from these programs are analyzed collectively later in this thesis to provide direction for further experimentation and the development of an analytical force model.

3.1 Pilot experiments for first-year ridge modelling[1]

In this section small-scale laboratory experiments modelling first-year ridge interactions with structures are described. Tests were aimed at determining the mode of failure of ice rubble accumulations under varying loading conditions and the stress levels required for failure. The packing density and shear behaviour of the laboratory ice rubble were also examined under varying conditions since these properties influence the strength of ridge keels and are necessary for model calibration. The first attempt to substitute sand for ice rubble as a modelling tool for studying keel rubble failure mechanics is also described.

3.1.1 Scope of experiments

Experiments were undertaken in the summer and fall of 1994 with the intention of replicating first-year ridge keel encounters with fixed offshore and coastal structures. For logistical reasons the experiments involved translating a rigid indentor (or model pier) into stationary ice rubble. This preserves the relative motions of the pier, rubble and water yet simplifies testing. The tests are designed to demonstrate the trends in failure mode and loads as control parameters are varied.

All experiments were conducted at C-CORE in a cold room at 0° C. Commercially available freshwater ice cubes were used for the tests. Floating accumulations of ice rubble were systematically indented by a mechanically driven, instrumented cylinder in the first test series. Similar procedures were used to test the ice rubble in a dry state, stacked on a false floor inside the tank. First-year ridges may reach depths of over 20

---

[1]A version of this section was prepared for K.R.Croasdale and Associates, sponsored by National Energy Board and titled *Bruneau, S.E (1994a) **Ice load models for first-year ridges and rubble fields** - physical laboratory tests*.

m so that hydrostatic pressure due to buoyancy can be high, up to 15 kPa as one approaches the waterline from the keel bottom. For a cohesive granular material (obeying linear Mohr-Coulomb failure criteria) the frictional shear resistance would be relatively high, theoretically three times cohesion if $c = 5$ kPa and $\phi = 45°$. It may be expected, however, that for accumulations of rubble at the laboratory scale, cohesion would dominate rubble shear strength since buoyant stresses are low. The "dry" tests, which effectively increase inter-block stresses by as much as an order of magnitude for similar sized accumulations, attempted to examine this effect. Pore fluid and boundary conditions also change the behaviour of ice rubble so that normal stress effects were not perfectly isolated in these experiments, considered exploratory in nature.

Overall dimensions of ridge keels and ratios were geometrically scaled at approximately 1 to 100 (for the case of the Northumberland Strait Crossing Project) but particle scaling and dynamic modelling (forces mainly) were not intended or achieved in the lab. The control parameters considered for the ice rubble indentation tests were the ice temperature upon placement, the rubble contact duration before indentation and the width and depth of the rubble accumulation.

Model "sand keels" were indented to demonstrate the potential for this approach to aid in ridge keel model development. The properties of silica sand are well-defined and some load formulas used in ridge keel modelling are geotechnical in origin. Thus it was postulated that sand tests, which are easier and faster to perform, would provide a meaningful analogue for ice rubble experiments. Furthermore, parametric control and observation capabilities are greatly enhanced.

A shear box apparatus was developed and used to determine the cohesive and frictional properties of the ice rubble studied, and, rubble porosity and repose angle were determined.

3.1.2 Apparatus

A steel tank one meter square at the top and 0.76 m deep was used in the study (Figure 3.1). Its heavy steel frame and rugged support legs provided a stable platform for the drive mechanism used in the indentation and shear tests. Two plexiglass windows (0.6 m square) were installed in the side and rear of the tank for underwater lighting and viewing. The drive mechanism was an assembly of aluminum and steel structural parts, a traversing block which rigidly supported the model indentors, a threaded lead screw and a stepper motor. The motor was controlled through a power supply unit by a Zenith 386 laptop PC supporting stepper motor software.

Data acquisition was handled through a 286 PC with a 10 V data acquisition card on board using **Snapshot** software. Two, 1.1 kN, waterproofed, cantilever load cells, on loan from the Institute for Marine Dynamics (IMD-NRC, St. John's), were used for load measurement. Using the two single axis load cells as model supports permitted the resolution of the resultant load. A "yoyo" displacement potentiometer was attached to the top of the drive mechanism to measure the absolute displacement of the traversing block relative to the tank frame. All experiments were recorded using a Super VHS recorder mounted on a high tripod beside the tank.

Ice and sand properties

Ice used in the studies was purchased from a commercial supplier of ice cubes. Unused,

the individual pieces were roughly cylindrical, concave at the ends and had a diameter of 25 mm and a length of 30 mm. The pieces changed shape after some use by losing sharp edges and concavity and some grading occurred through agglomeration and splitting. The ice temperature during testing ranged from -24° to 0.0° C.

Subangular silica sand type 'O' with a dry weight of at 13880 N/m^3 was used for all sand tests. The internal friction angle at this specific weight is around 32 degrees and the effective grain size is 0.325 mm (Paulin, 1992).

3.1.3 Structure interaction experiments with ice rubble and sand

Floating ice rubble indentation experiments

Air, water and ice temperatures were recorded before each indentation test. The placement time and test time were also taken so that static contact duration of the bulk ice rubble samples was known. Ice stored in a deepfreeze was removed and mechanically separated by striking and applying pressure to the containment bags. This ensured that all freeze-bonds between ice pieces were broken prior to placement in the tank support frame. After a few moments the central gate section of the support frame was removed to provide a clear path for the model structure (Figure 3.2). The remainder of the frame acted as a rigid (moment-bearing) connection for the ice formation adjacent to the exposed area. The indentor was computer-controlled to advance at a rate of 6 mm/s with a 2 mm/s^2 acceleration and deceleration at the beginning and end of each test. The motor drive was stopped at a prescribed distance into the rubble. The deformed rubble accumulation was observed after each test and a recording of the unloading process was made. The support frame was partially removed from the tank to allow access to the ice

rubble for removal, drainage, bagging and storage.

With the exception of calibration files all experiments were recorded digitally at 50 Hz for a 120 second interval and later lowpass filtered digitally at 3 Hz. The calibration coefficients determined in a pretest calibration experiment were applied to each of the raw voltage data time series. A time channel was established and the results from the two load cells were added to establish a 5 channel data file of the calibrated data time series. After plotting the complete series for each test the exact starting point for the indentation was found and the first 60 seconds of each test was isolated.

Nine floating ice rubble indentation experiments were recorded as listed in the table in Figure 3.3. The settings for the first two experiments represented the default values of the control variables. Tests were performed to determine the sensitivity of load and failure mode to ice temperature and contact duration, rubble depth, rubble width, and support boundary conditions. Since the temperature of the ice after placement in the water was not measured the residency of the ice in the tank (at 0° C) is given.

The table also lists the maximum force on the pier model during the first 60 seconds of each test and the failure modes observed. The bar chart in Figure 3.3 indicates the relative influence of the control parameters. From this figure some trends in measured forces emerge:

- load is highly sensitive to rubble depth,
- warmer ice rubble results in reduced strength,
- the width of the rubble accumulation influences indentation resistance,
- continuous "rubble fields" have greater resistance than discrete "ridges", and

- rubble shear resistance increases with contact duration.

Additional analysis indicated that over the first 60 seconds maximum loads were, on average, double the mean loads for both discrete rubble and continuous rubble accumulations while the standard deviation was between 1/4 and 1/2 the mean.

The load traces for tests RF012 and RF08 are shown in Figures 3.4 and 3.5. These traces are representative of the indentation of discrete (ridge-like) and continuous (rubble field-like) accumulations. Failure modes observed on video records were synchronized with force records and are summarized on each figure.

The plug failure observed in the floating ice rubble tests is generally preceded by some local failure. A few tests saw plugs form simultaneously with first ice contact. Most often, however, the indentor was embedded in the rubble formation when the plug forms. On average plug movement started when the indentor penetrated 12% of the rubble width. The geometry of the plug varied considerably. Often failure planes flared tangentially from the pier model outwards towards the support points at the rear of the rubble mass. Occasionally though straight shear planes formed between fore and aft support points leaving much of the ice around the indentor undisturbed. Usually, the plug tended to advance in stages as it remained partially interlocked with the rest of the ice.

The local (non-plug) failure mechanism was characterized by an upward shifting of ice pieces which formed a raised elliptical crescent around the indentor. Some large scale shifting of rubble in the outer reaches of formation were observed. The raised ice formation extended out in front of the indentor approximately the depth of the ice but

tapered around the sides and fell off to below level ice grade and ultimately to water level behind the indentor. The depth of the pile-up at the highest point was approximately 2-4 cube widths above level ice grade.

At least three dynamic load mechanisms (or load release mechanisms) were recognised in all load traces. The highest frequency appears to correspond to the repositioning of individual ice pieces within the coherent formation. Clumps of ice rubble periodically shift in the vicinity of the indentor leading to lower frequency events. The lowest frequency corresponds to the global repositioning of bulk rubble blocks during plug-like failure.

Dry ice rubble indentation experiments

A series of eleven "dry" ice rubble indentation tests were conducted in the tank in the C-CORE cold room. A false floor made of high density polyethylene and a new, shorter pier model were placed in the tank after water was removed. The pier was positioned so that it swept over the smooth plastic floor with a spacing of 6 mm throughout. Ice rubble was placed on the floor in a fashion similar to the tests performed in water using the same holding pen and positioning system. Ice temperature, rubble depth and the slope of the leading and trailing edge of the accumulations were varied. Indentation rate was 6 mm/s.

The table in Figure 3.6 lists the conditions under which the tests were performed. Load traces for test DR03, for a "ridge-like" formation and DR05, for a "rubble field-like" formation are shown in Figures 3.7 and 3.8. The two traces reveal distinctly different force patterns which also correspond to dissimilar failure modes observed during testing.

Trends in peak loads observed in Figure 3.6 are essentially the same as those for floating rubble when similar control parameters are varied. Some of the "dry" rubble test results are as follows:

- load is sensitive to rubble depth and sectional area,
- warmer ice rubble results in reduced strength,
- continuous "rubble fields" have greater resistance than discrete "ridges", and
- rubble shear resistance increases with ice contact duration.

The maximum loads for both discrete ridge and continuous rubble tests were roughly double the mean and the standard deviation was very near 1/2 the mean. Uniform cyclic loading was observed in tests DR01, DR02, DR10 and DR11. This corresponded to a ratchet-like advance of the indentor, originally believed to be lock-in resonance at the structure fundamental mode. However, further inspection of the time histories revealed that cycles were around 1.7 Hz - one-tenth of the fundamental frequency of the structure. Thus it is more likely that the dynamic loading is a complicated interaction between the ice and the structure, controlled by advance rate, structural stiffness, and ice extrusion processes associated with creep, compressibility and crushing strength.

Plug failure geometry and movement was difficult to observe in the "dry" tests. The ice shifted in quick steps making it difficult to discriminate where failure planes had formed. It appeared that rubble movement occurred across a flaring wedge shaped rubble block which leads the indentor. The first plug movements were noticed 30 seconds into the indentation at 180 mm or 40% of the rubble width on average. The local (non-plug) failure mechanism may be characterized as a cyclical rearrangement, lifting and translation of clumps of ice pieces. The raised formation was elliptic and tapered. The

depth of the pile-up was approximately 2-4 ice cube diameters.

Maximum forces in the "dry" tests were anywhere from 2.5 to 10 times greater than those in similar floating rubble tests where the ratio of dry weight to buoyant weight was approximately 11. Assuming loads from inertia, fluid dynamics and floor friction to be relatively low, one would expect little difference between indentation forces for wet and dry tests if the rubble were purely cohesive. Also, if the rubble were purely frictional then the indentation forces should be proportional to normal forces, *i.e.* weight. Since results are somewhere in between one may infer that both properties act, though the probable dependency of ice rubble cohesion on confining stresses complicates this interpretation.

Sand indentation experiments

Experiments on damp sub-angular silica sand were performed utilizing the apparatus as configured for the dry ice tests (Figure 3.9). Figure 3.10 lists and illustrates the results for the four "sand keel" tests performed. Loads appear to be directly proportional to the sectional area of the "sand keels". Plug failure occurred approximately 30% of the way through the pile widths though the ratio is probably a function of sand depth, width and structure diameter. The continuous sand layer yielded the highest resistance - a 30% increase over the others. Figure 3.11 indicates that the load levels and patterns at penetrations up to 30% of keel width were the same for all tests, which supports the basis of the *cross-over* modelling approach as described in Section 2.4 and illustrated in Figure 2.10 (where peak loads occur at local and plug failure transition). The three plug failure force traces are remarkably similar to the force trace DR03 for a similarly shaped "dry" ice rubble accumulation. The pattern is again seen in the first 20 seconds of

RF012, a floating ice rubble experiment. This is evidence that gross failure modes for sand are somewhat representative of those for ice rubble.

Failure patterns easily distinguished in the damp sand are sketched in Figure 3.12 for test SA02. The local plastic deformation of the sand was characterized by an uplifted area of sand that increased in height, broke and was divided as the indentor approached and passed. In the slightly damp sand there was a tendency for the sand to terrace as repeated passive failures occurred.

The origins of the plug failure shear planes were not distinctive but appeared to be within the compressed passive failure zone adjacent to the indentor. The planes propagated outward towards the far side of the sand formation breaking at an increased angle near the free edge. They did not appear to be vertical planes nor did the sand within the plug translate uniformly. The leading edge of the plug fanned out, cracking and falling in height. The entire plug appeared to slide on the plastic floor so that sand did not remain in the rear path of the structure.

3.1.4 Shear box experiments

The shear strength of the ice rubble used in the indentor tests was investigated. Both normal stress and ice temperature at placement were controlled so that Mohr-Coulomb yield criteria could be established for different temperature regimes. A shear box was fabricated from heavy polyethylene and PVC as shown in Figure 3.13. The experiments involved placing ice rubble into the shear box which was positioned in the water so as to allow neutral buoyancy of the ice when the box was full. The top shear ring of the box was pulled horizontally by a load cell on the traversing block at 1 mm/s relative to the

stationary bottom ring.

Eighteen tests were performed in which ice temperature, contact duration and normal stress were controlled. Five tests were performed without any ice to monitor and calibrate the friction of shear box mechanism, before and after tests. All test results have been corrected for no-load box friction.

The maximum shear stress in the first 60 seconds for each test is listed in the table in Figure 3.14. Sample force time-histories are shown in Figures 3.15 and 3.16 for SB08 and SB14.

Load traces for the shear box exhibited 2 scales of load and release. The first at high frequency and low load amplitude (1-30 N and 1-5 second periods), the second at low frequency and high load amplitude (hundreds of Newtons at 25 second periods). The small force fluctuations probably resulted from incremental shifts in ice pieces as the rubble mass was compressed. The large fluctuations resulted from the global shearing of the bulk rubble sample. With interest it is noted that the dominant low frequency high load cycle occurs at a displacement approximately equal to one ice cube diameter (25 mm). The predominant shape of this load trace is saw-toothed with the load drop occurring earlier in tests with lower normal pressure (surcharge).

Shear strength was calculated from the first peak before a major drop in load. In a few tests secondary cycles achieved higher loads but may have involved jamming so these results were not considered. The normal stress was determined by adding the buoyant weight of ice beneath the shear plane to the steel weights and plastic platen used for surcharge, and then dividing the sum by the original cross sectional area of the shear

box.

Figure 3.14 shows the plots of maximum shear stress versus normal stress for both cold and warm ice rubble in the lab. The Mohr-Coulomb approximation is shown for each. Values fall in the range of those reported in the literature as described earlier. The friction angle was similar for tests with warm and cold ice (54° and 59°). Cohesion, on the other hand, appeared to be significantly affected by the temperature of the rubble with an apparent threefold increase for colder ice (720 to 2460 kPa).

3.1.5 Ice rubble repose angle experiments

Repose angle experiments were aimed at detailing the influences of ice rubble temperature and block shape on repose angle (Figure 3.17). Ice was piled lightly with a scoop into a mound centred around a vertically positioned measuring rod. Ice used in these tests fell into three categories; dry unused ice cube rubble from the deepfreeze ($\approx$ -21 C), previously used (in the wet tank) rubble also taken from the deepfreeze, and warm ice (0 C) which was used in wet tank experiments. After five trials with each sample the cold, new ice (the most angular of all) exhibited the steepest repose angle at 36°. The warm ice averaged an angle of 34° and the cold used ice was measured at 33° on average. Repose angle is often considered a lower bound estimate of the internal angle of friction for cohesionless soils (Bowles, 1985).

3.1.6 Ice rubble porosity experiments

The bulk porosity (volume of voids to total volume ratio), e, of the ice used in the experiments was determined in both dry and submerged states. To determine the ratio of the volume of ice to the bulk volume of a sample (1-e), a large container of known

volume was loosely filled with experimental ice and weighed. The volume of ice was determined from the measured weight assuming an ice density of 919 kg/m^3. The ratio of open volume to the total volume of the container was then determined. Results are shown in Figure 3.18. Ice that had been previously used in wet tests had 36% porosity while new, unused (more angular) ice was around 44%. Ice taken directly from the tank in a wet state had a porosity of around 39%.

In an effort to determine the porosity of floating ice rubble *in situ*, a large plastic container of known volume was placed in the test tank so that it was approximately 80% submerged. The bottom and sides of the container had been perforated with 5 mm holes so as to allow the free flow of water. Ice was added to the container until it was completely filled - apparent when ice obscured the visibility through the lower holes in the container wall. With the ice flush across the top, the container was slowly removed allowing complete drainage of the sample. The porosity was then determined (through weighing and volume calculations) to be 29%.

The drop in porosity for the "submerged" ice rubble was unexpected since it was anticipated that ice deposited in water would be subject to lower normal stresses leading to a decreased packing density. This may, however, have been more than offset by both the mode of deposition (always added from the top and pushed down), the melting of asperities and the fact that the ice used in this test had been utilized in other experiments and may have been somewhat graded. The bonding of some blocks and breaking up of others in prior experiments would lead to a tighter packing arrangement than new, sorted ice rubble.

3.1.7 Summary of C-CORE pilot test series

The resistance to indentation of floating laboratory ice rubble accumulations increased non-linearly with rubble depth, decreased with rubble width and decreased with higher ice temperature (at time of placement). Continuous rubble indentation resulted in higher loads than discrete "ridge-like" indentation. Plug failure occurred 12% of the way into the rubble formation on average. The plug geometry varied considerably as shear planes formed in parallel, flared and curved patterns for different tests. Maximum loads were on average double the mean and standard deviations were between 1/4 and 1/2 the mean for the first 60 seconds of the tests.

"Dry" ice rubble indentation test loads decreased with rubble sectional area, increased with decreased ice temperature at placement and increased when plug failure was not permitted (continuous rubble layer over discrete ridge tests). Loads were 2.5 to 10 times greater that similar tests on floating rubble (the ratio of effective weights being 11). Plug failure occurred 40% of the way into the rubble formation on average. Mean loads were approximately 1/2 the maximum and standard deviations were 1/2 the mean.

Indentation tests on "sand keels" yielded smooth load traces and highly reproducible results. The two failure mechanisms, local passive and global plug-like, were easily distinguished in the force-time histories and video records. Plugs were "bell" shaped and occurred 30% of the way into the formation. Similarities between "sand keel" force trace patterns and those for ice rubble supported the hypothesis that sand may be used as a modelling tool for looking at failure modes of ice rubble.

Shear box experiments on floating ice rubble demonstrated the sensitivity of rubble shear

strength to ice temperature at the time of submergence. Mohr-Coulomb criterion established from the shear box tests produced friction angle values of 59° and 54°, and cohesion values of 720 Pa and 2460 Pa for warm and cold ice respectively. Tests also revealed two scales of load cycling in the force traces. The first was a high frequency low load event, the second was a low frequency and high load event occurring at a displacement around one ice block diameter.

The repose angle of the lab ice varied from 36° when cold and angular, to 33° when cold and used. Ice rubble porosity varied from wet to dry states and with the degree of prior use. Values ranged from 44% porosity for highly angular, cold, dry ice to 29% for submerged, used ice.

The physical laboratory tests described have demonstrated that the shear resistance and structural strength of ice rubble at laboratory scale are highly influenced by the temperature of ice upon placement (whether it is submerged or not), normal stresses, residence time (in a static position), and to a certain degree the geometry of the lab ice pieces and boundary conditions. The geometries of plug and local passive failure surfaces are complex and somewhat random. Sand provided a useful tool for demonstrating force trends and failure modes and may provide the simplest approach for parametric investigations of other ridge keel failure properties.

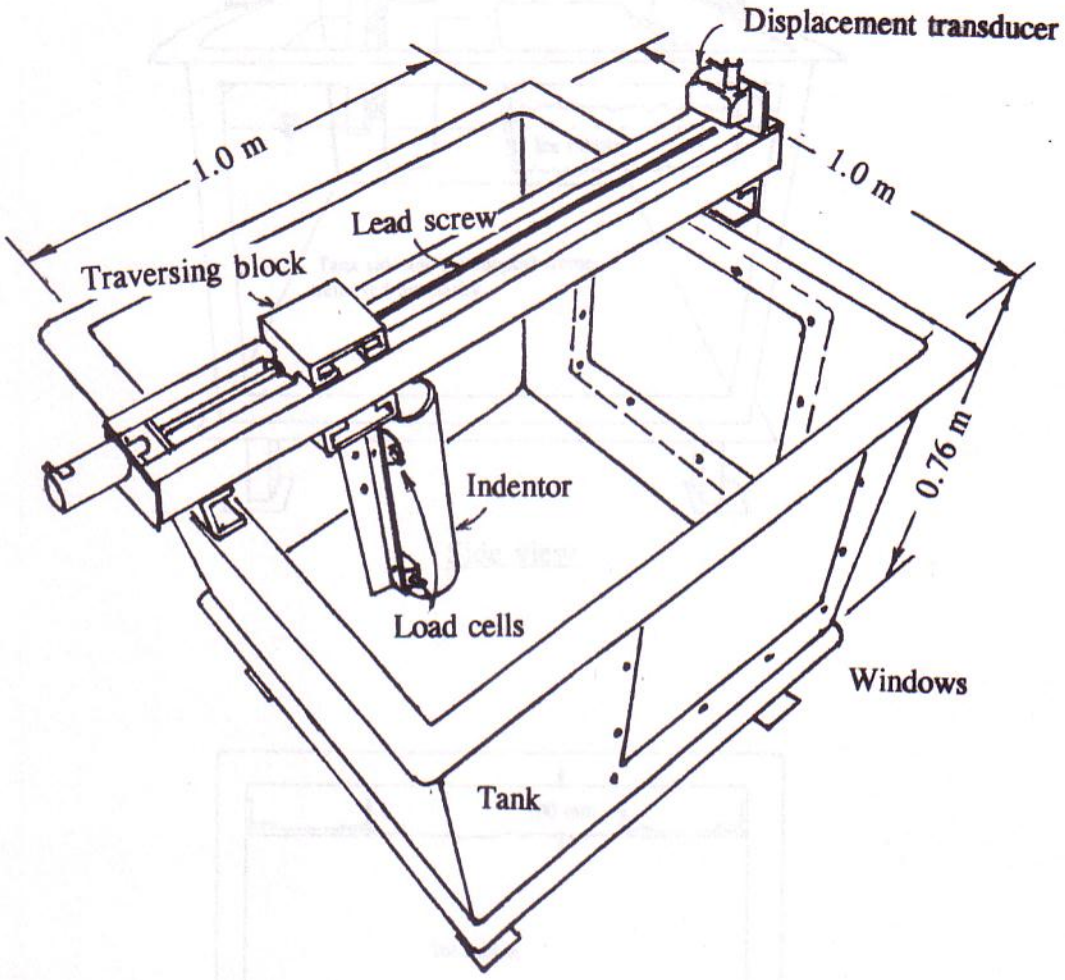

Figure 3.1 Oblique view of apparatus.

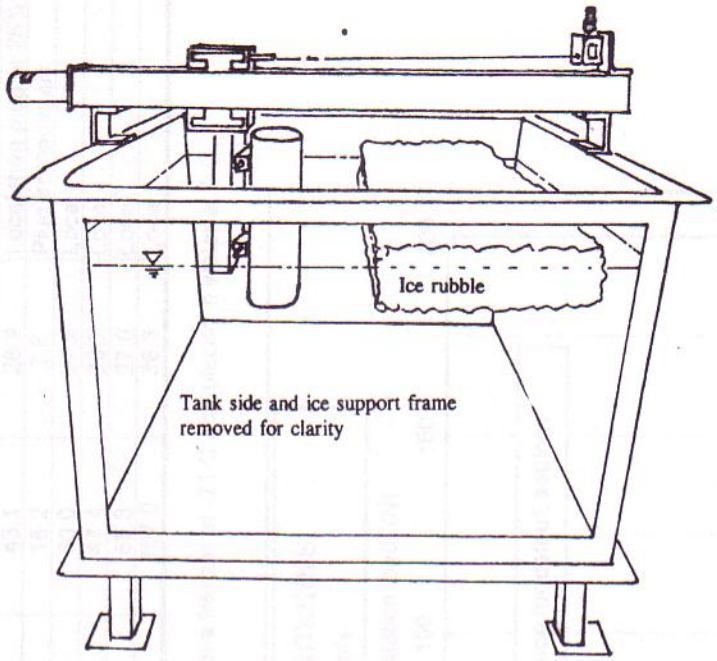

Side view

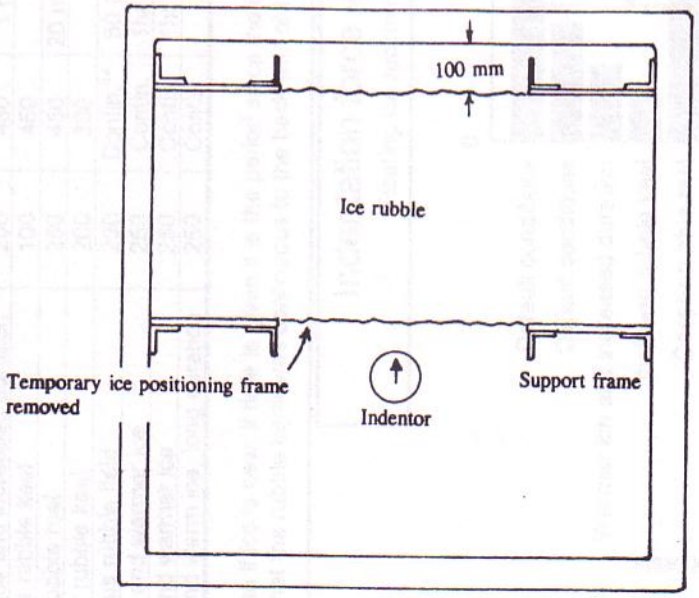

Plan view

Figure 3.2 Setup for floating "wet" ice rubble experiments.

Test	Test description	Ridge depth mm	Ridge width mm	Ice temp/ condition*	Duration in frame min.	Max force (first 60 s) N	Mean force (first 60 s) N	Failure modes observed
RF01	Default conditions	200	450	-24 C	7	40.0	n/a	Local then plug at 25%wid
RF012	Default conditions	200	450	-24 C	7	30.1	18.0	Immediate plug
RF04	Warmer ice and increased duration	200	450	1 hr in tank	30	19.6	13.1	Mixed: local and plug
RF02	Shallower rubble keel	100	450	-24 C	8	10.7	6.2	Mixed: flexure and plug
RF06	Deeper rubble reel	250	450	20 mins& -24C	7	43.1	26.9	Local then plug at 25%wid.
RF03	Narrower rubble keel	200	300	-24 C	7	16.2	7.8	Plug immediately
RF05	Continuous rubble field	200	Contin.**	50 & 30 mins	8	60.0	27.9	Local
RF07	Contin.** and warmer ice	250	Contin.	1hr &10 mins	10	47.4	20.7	Local
RF08	Contin. and warmer ice	250	Contin.	1hr &30 mins	9	55.3	27.0	Local
RF09	Contin. and warm ice, long duration	250	Contin.	21 hrs	1140	167.0	36.3	Local

* Temperature given if ice is new, if time is given it is the period since the ice was removed from a freezer at -21 C and placed in water at 0 C.
** Contin. means that the rubble layer was continuous to the back wall of the tank.

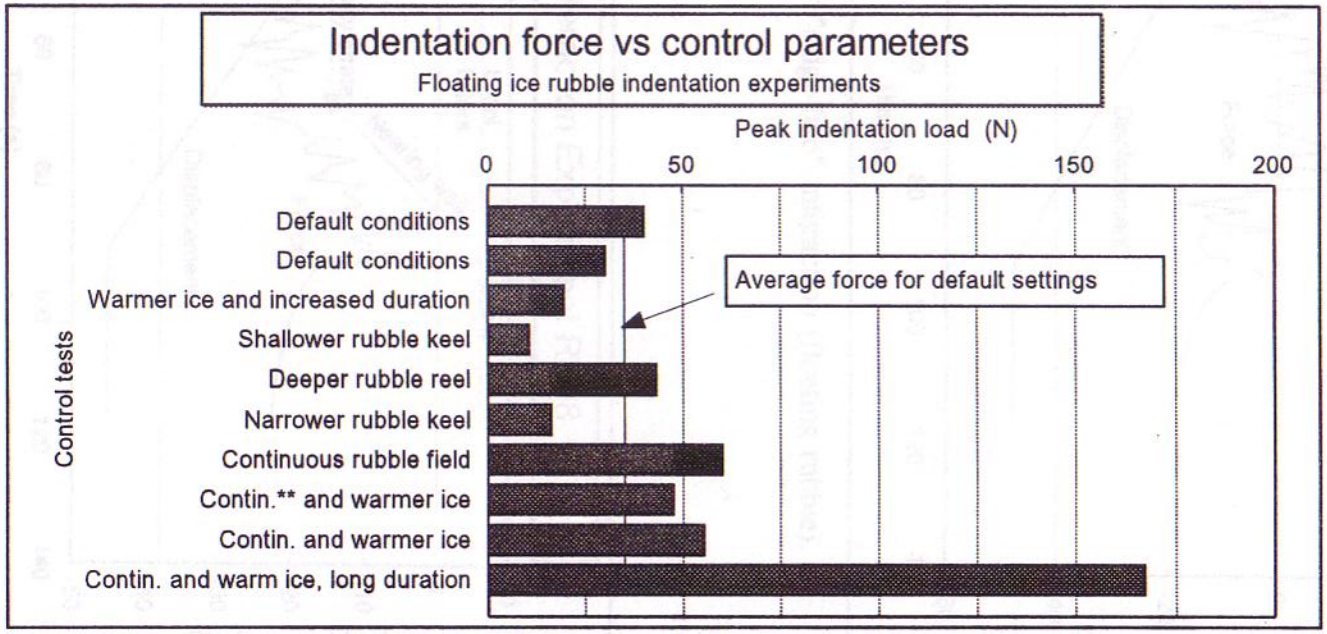

Figure 3.3 Floating ice rubble test conditions and results.

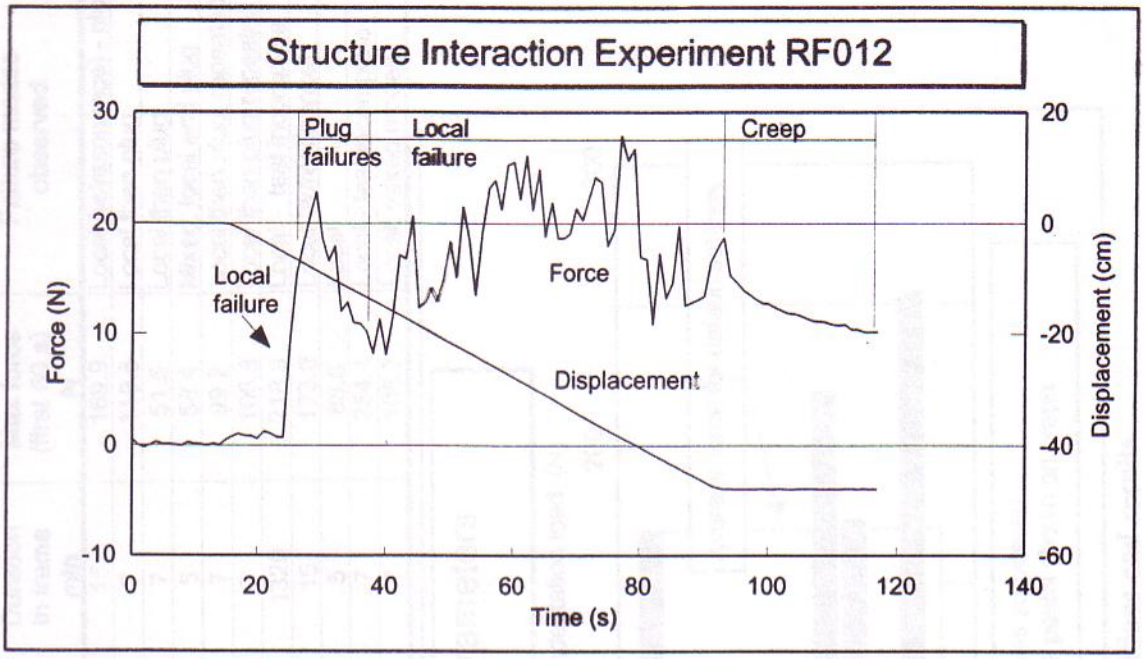

Figure 3.4 Force trace for "ridge-like" interaction (floating rubble).

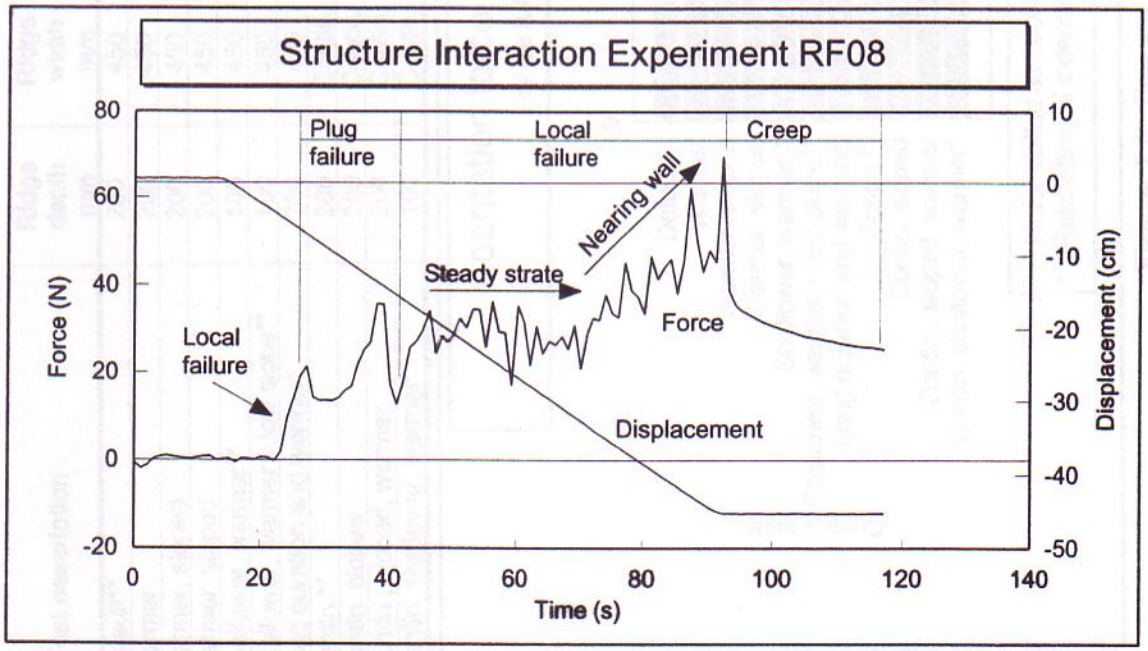

Figure 3.5 Force trace for "rubble field-like" interaction (floating rubble).

Test	Test description	Ridge depth mm	Ridge width mm	Ice temp./ condition	Duration in frame min	Max force (first 60 s) N	Failure modes observed
DR01	Default**	200	450	-24 C	15	169.9	Local (w/resonance) - plug
DR03	Warmer	200	450	3 hrs @ 0 C	7	119.6	Local then plug
DR04	Warmer, sloped	200	450	3 hrs @ 0 C	7	51.5	Local then plug
DR06	Warmer, sloped	200	450	4 hrs @ 0 C	5	58.4	Mixed: local and plug
DR10	Shallower, warmer**	100	450	27 hrs @ 0 C	7	99.2	Local then plug, repeated
DR11	Shallower, warmer v.low slope**	100	450	27 hrs @ 0 C	7	106.8	Local then plug repeated
DR07	Long duration and warmer*	200	450	26 hrs @ 0 C	1320	218.9	Local - test incomplete
DR02	Contin.**	200	Contin.	-24 C	15	173.0	Local (w/resonance)
DR05	Contin. sloped	200	Contin.	4 hrs @ 0 C	5	88.6	Local
DR06	Contin., sloped, warmer	200	Contin.	26 hrs @ 0 C	7	254.4	Local - test incomplete
DR09	Contin. shallower, warmer*	100	Contin.	26 hrs @ 0 C	7	106.7	Local: mixed modes

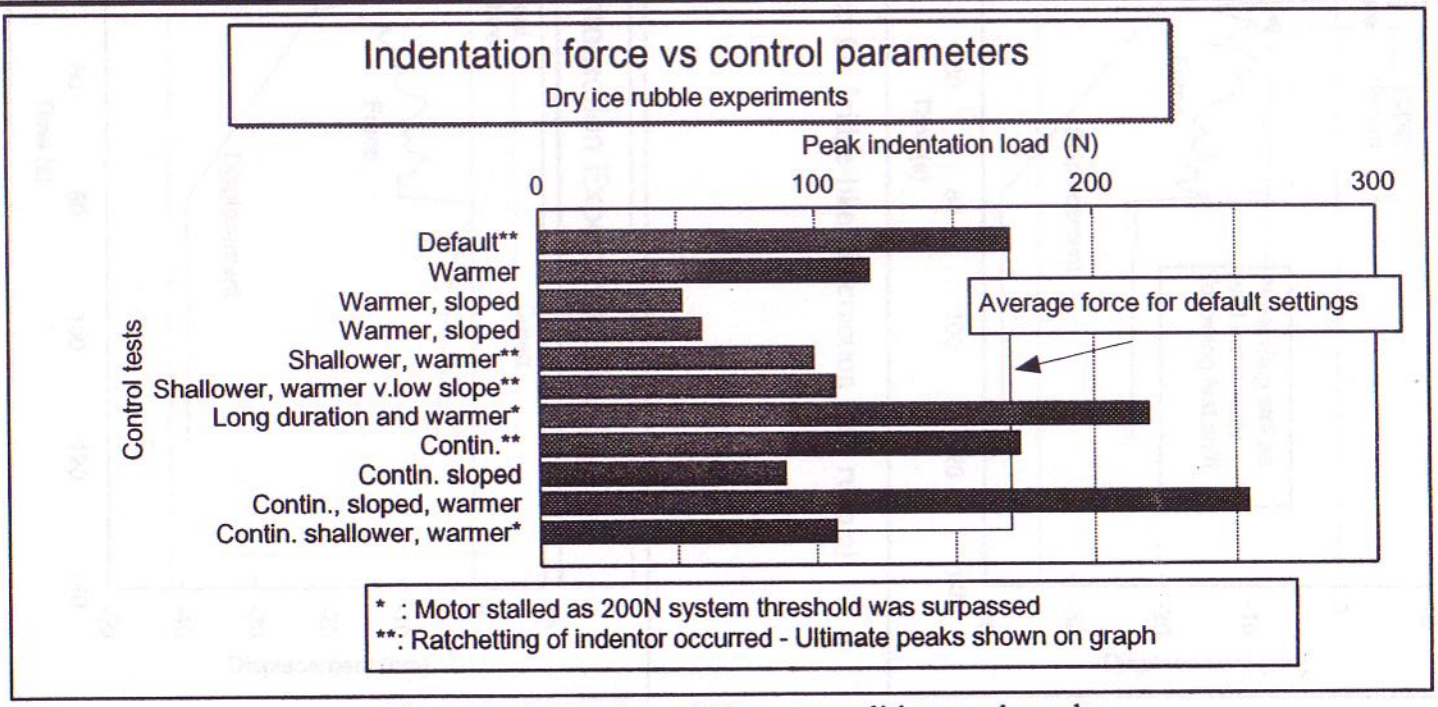

Figure 3.6 Dry ice rubble test conditions and results.

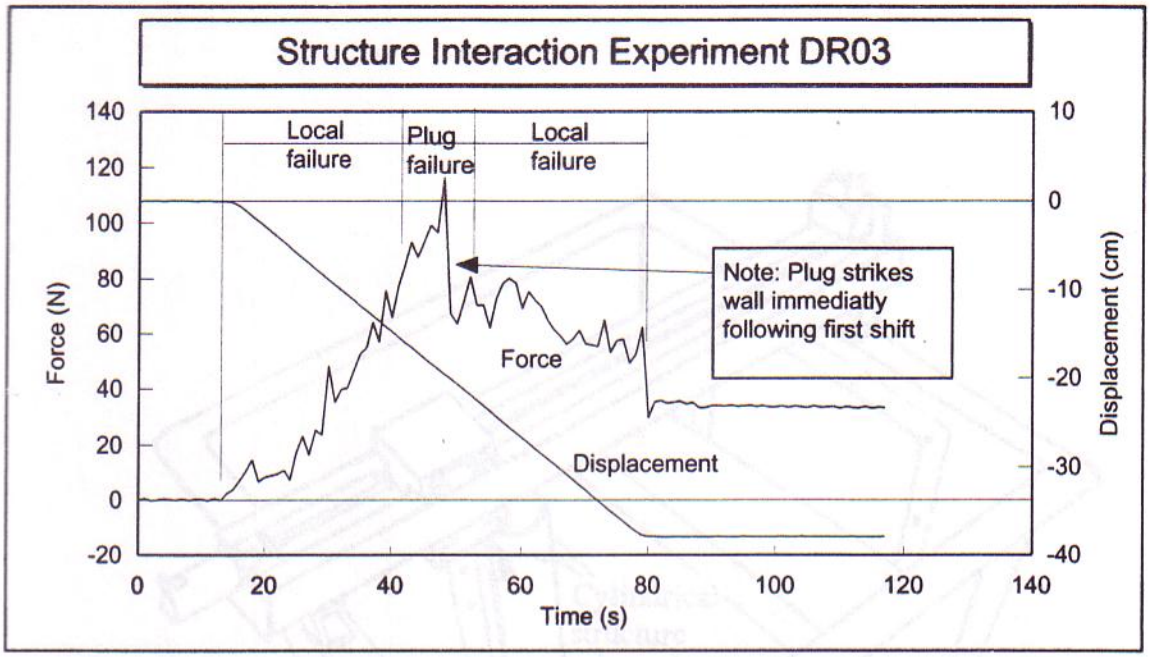

Figure 3.7 Force trace for "ridge-like" interaction (dry rubble).

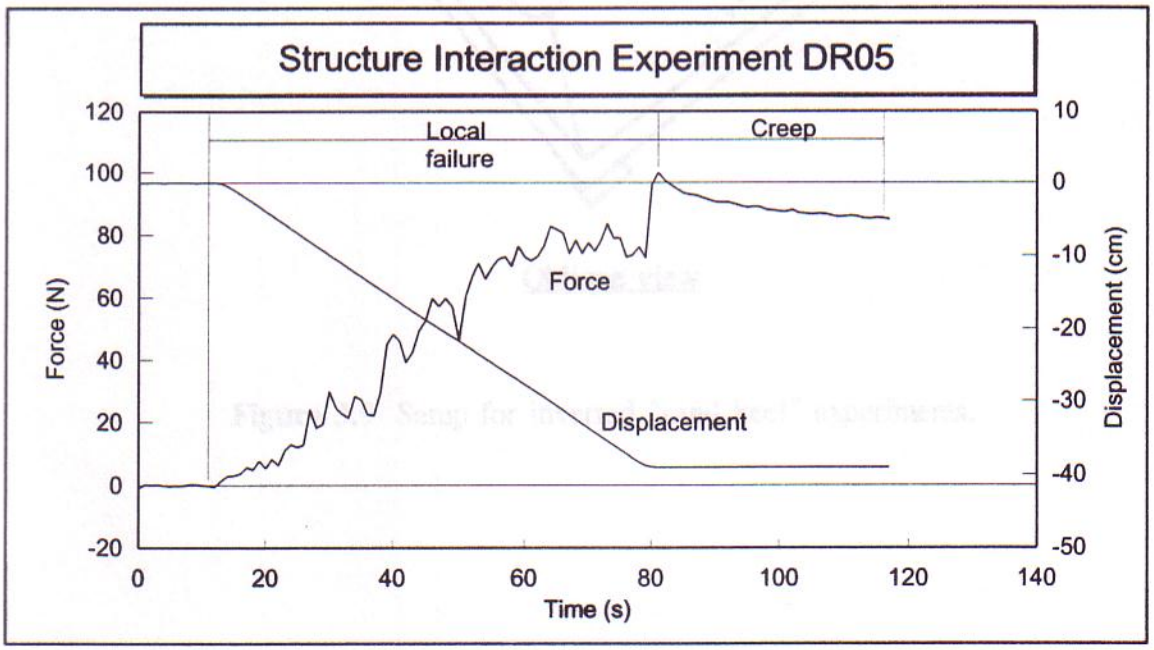

Figure 3.8 Force trace for "rubble field-like" interaction (dry rubble).

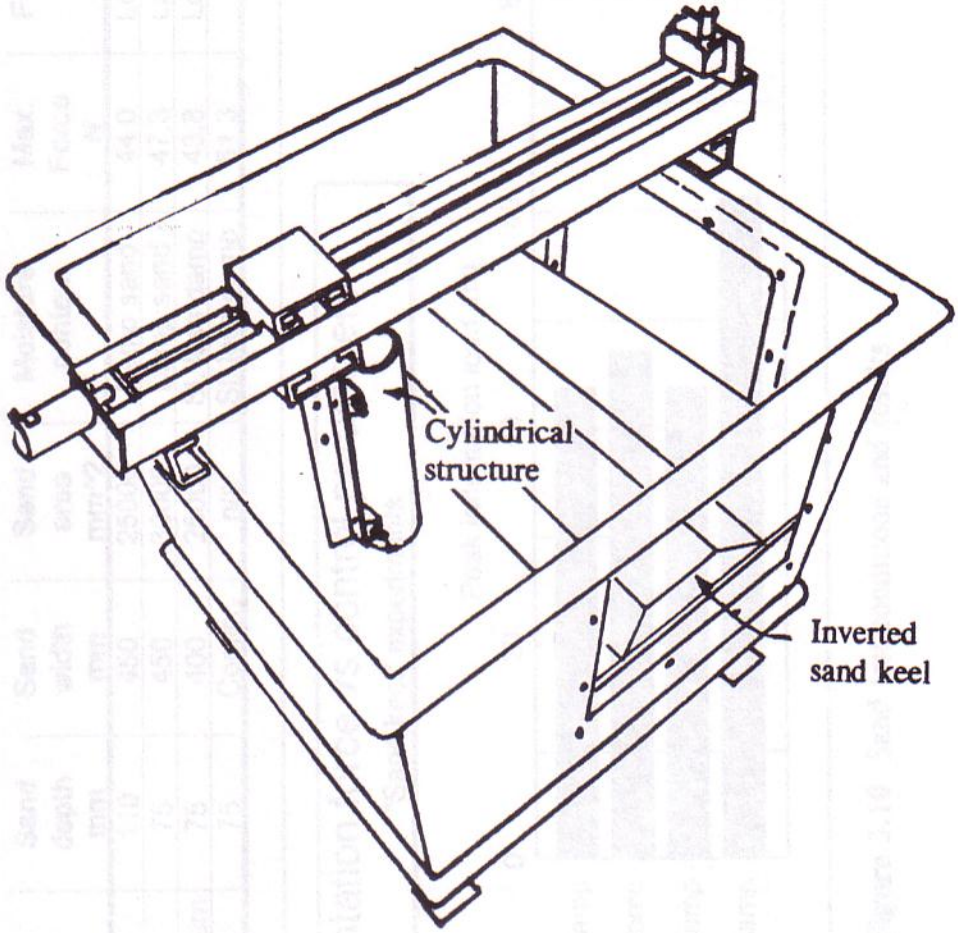

Oblique view

Figure 3.9 Setup for inverted "sand keel" experiments.

Test	Test description	Sand depth mm	Sand width mm	Sand area mm^2	Moisture content	Max. Force N	Failure modes observed
SA01	Triangle, damp	110	450	25000	Damp sand	44.0	Local then plug
SA02	Trapezoid, damp	75	450	30000	Damp sand	47.3	Local then plug
SA03	Trapezoid (narrower), less dam	75	400	25000	Sl. less damp	43.8	Local then plug
SA04	Continuous, less damp	75	Contin	n/a	Sl. less damp	61.3	Local

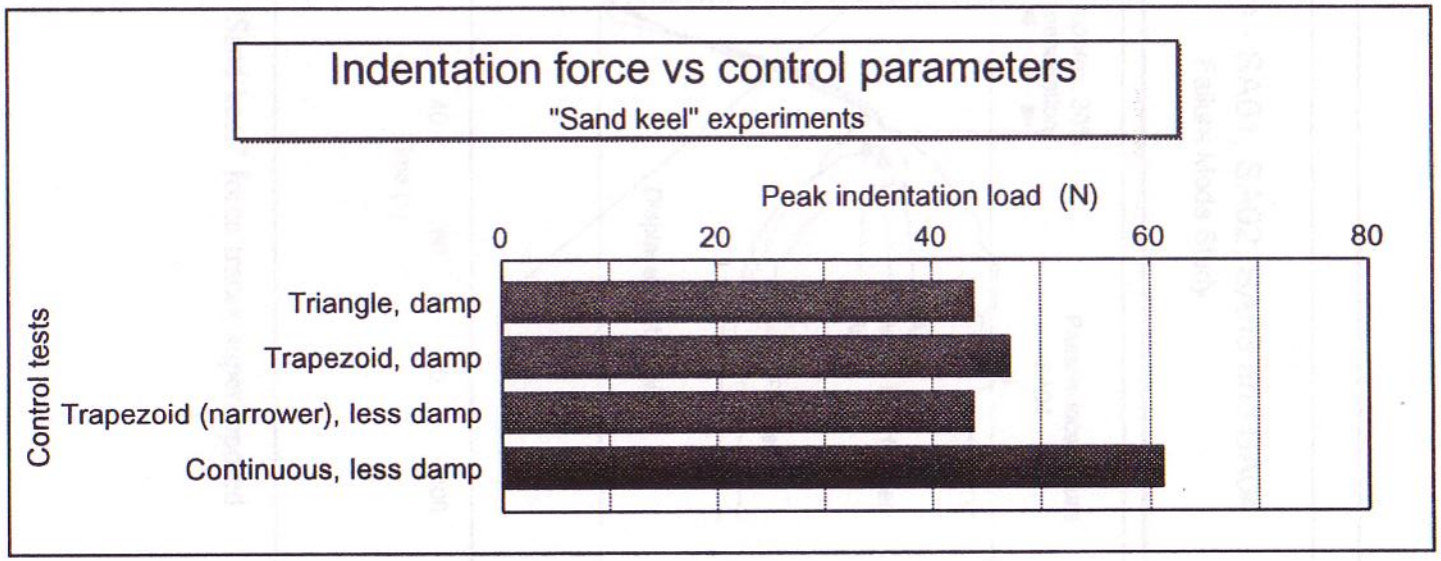

Figure 3.10 Sand test conditions and results.

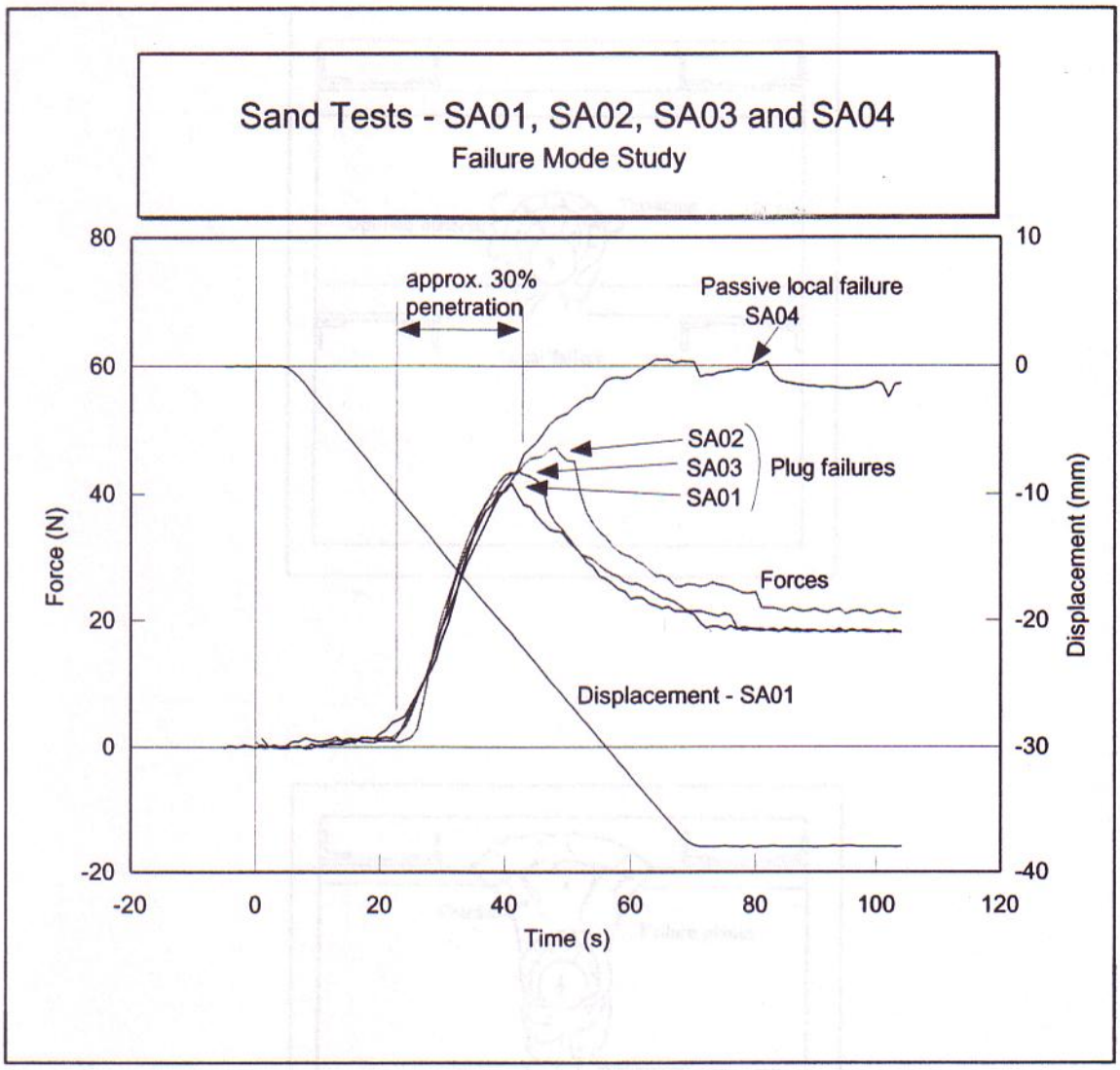

Figure 3.11 "Sand keel" force traces superimposed.

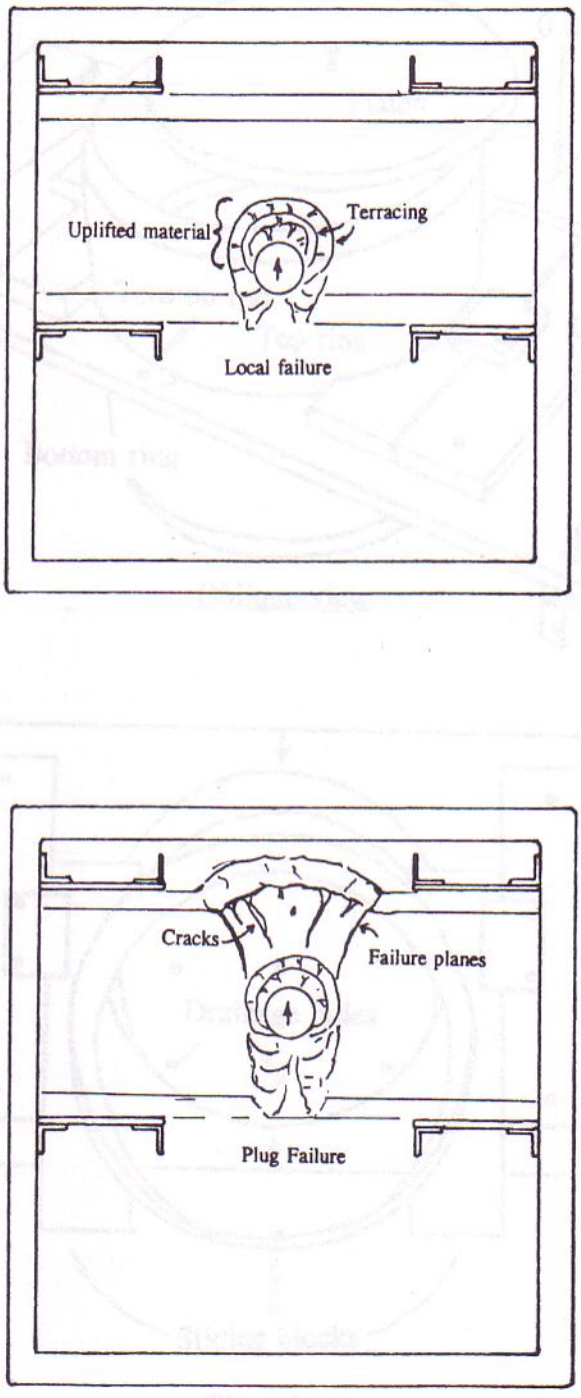

Figure 3.12 Failure patterns in an indented "sand keel" (SA02).

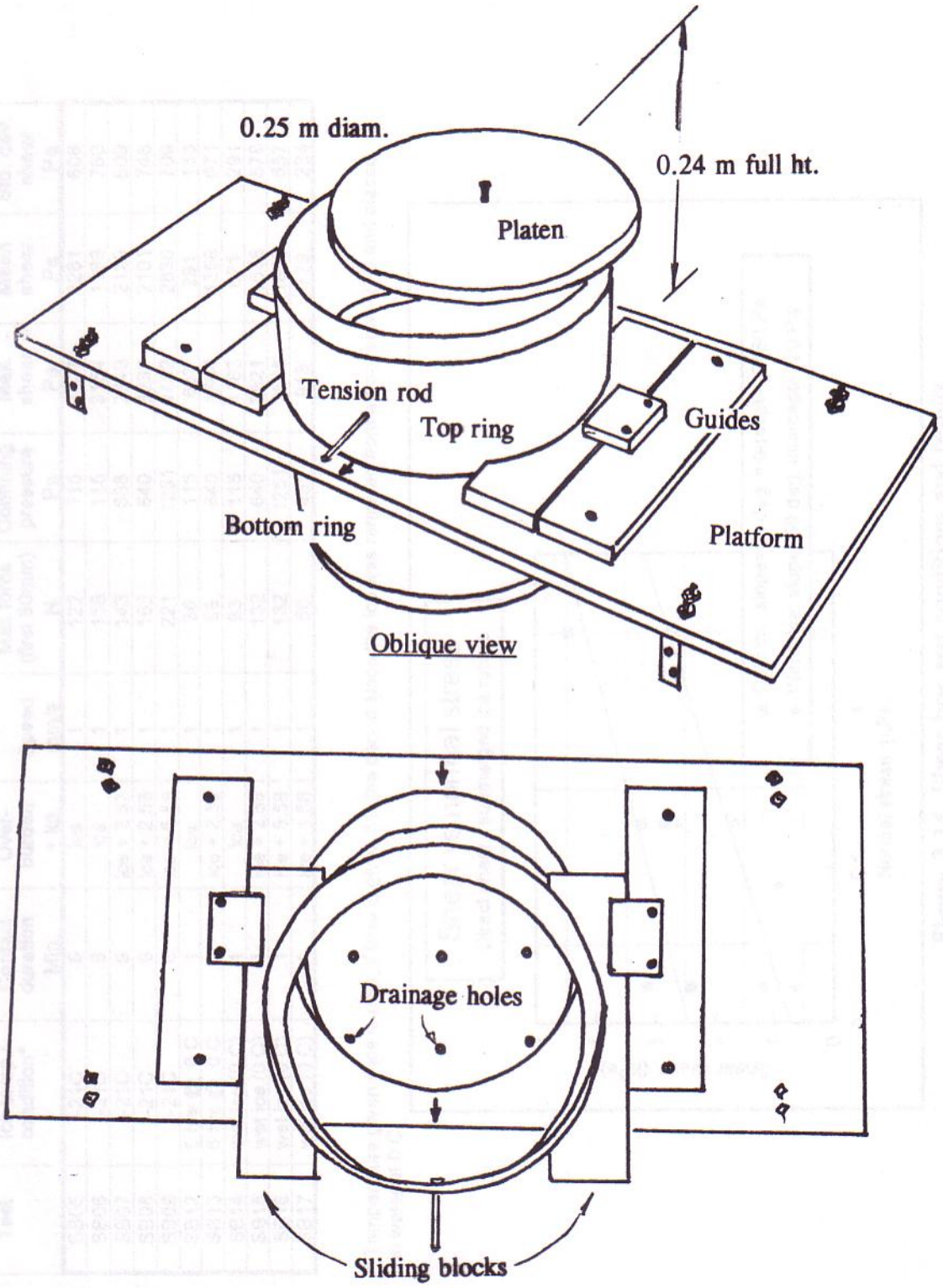

Figure 3.13 Polyethylene shear box for ice rubble.

Test	Ice temp./ condition*	Contact duration Min.	Over-burden + kg	Speed mm/s	Max force (first 60mm) N	Confining pressure Pa	Max. shear Pa	Mean shear Pa	Std. dev. shear Pa
SB05	-21C	6	ice	1	122	115	2407	1281	608
SB06	-21C	6	ice	1	158	115	3154	1989	760
SB07	-21C	6	ice + 2.57	1	143	638	2849	2129	609
SB08	-21C	6	ice + 2.58	1	162	640	3237	2101	746
SB09	-21C	6	ice + 5.58	1	221	1251	4452	2830	709
SB12	5 hrs @ 0 C	1	ice	1	36	115	633	291	133
SB13	5 hrs @ 0 C	1	ice + 2.58	1	86	640	1660	1356	671
SB14	wet ice (0 C)	1	ice	1	63	115	1183	671	291
SB15	wet ice (0 C)	1	ice + 2.58	1	132	640	2621	1556	576
SB16	wet ice (0 C)	1	ice + 5.58	1	132	1251	2605	1883	557
SB17	wet ice (0 C)	1	ice + 1.58	1	50	437	913	779	234

* Temperature given if ice is new, if time is given it is the period since the ice was removed from a freezer at -21C and placed in water at 0 C.

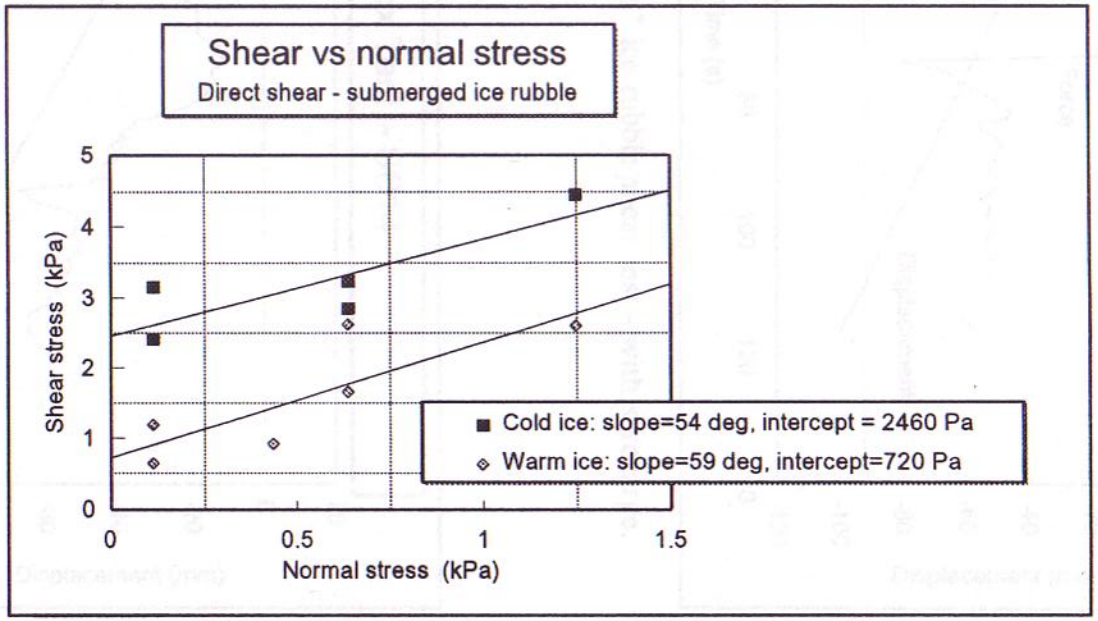

Figure 3.14 Shear box test conditions and results.

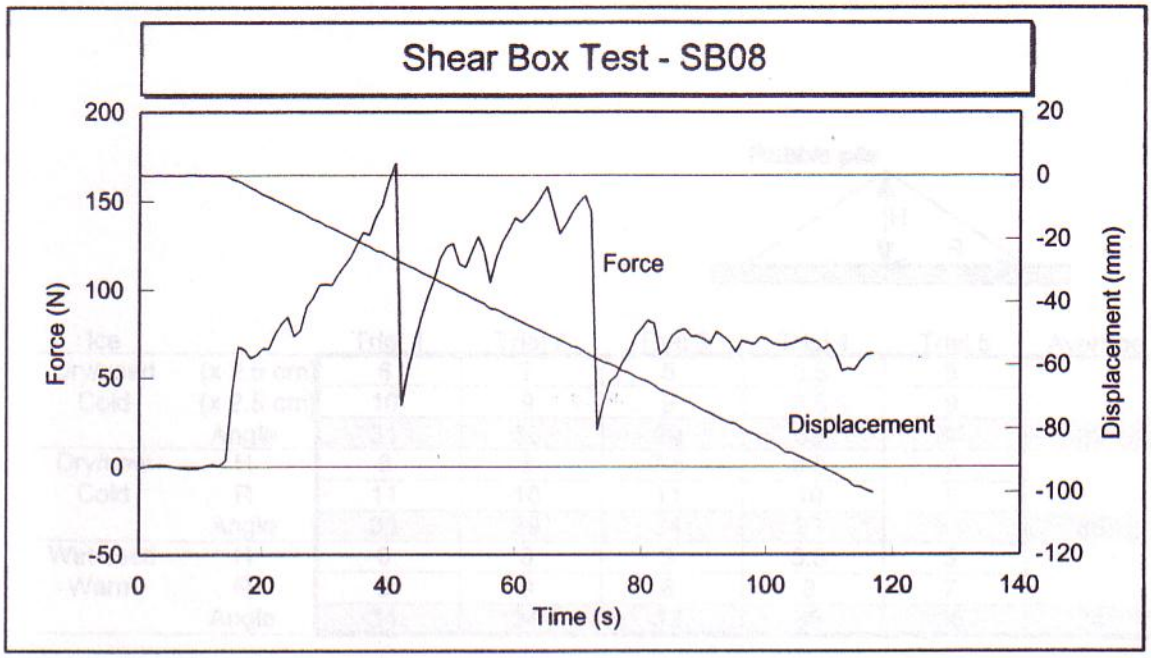

Figure 3.15 Force trace for "cold" ice rubble shear test - with surcharge.

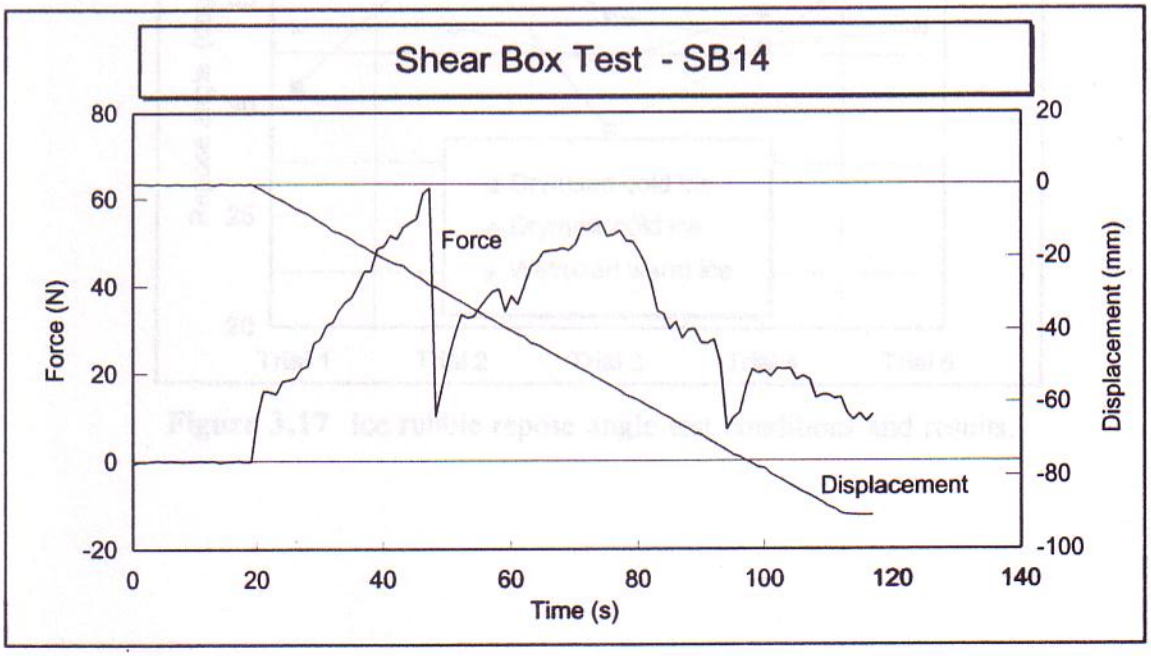

Figure 3.16 Force trace for "warm" ice rubble shear test - without surcharge.

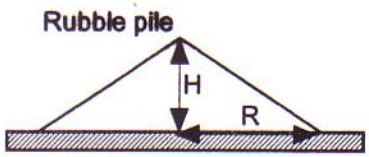

Ice		Trial 1	Trial 2	Trial 3	Trial 4	Trial 5	Average
Dry/used	(x 2.5 cm)	6	7	5	5.5	6	
Cold	(x 2.5 cm)	10	9	9	8.5	9	
	Angle	31	38	29	33	34	33
Dry/new	H	8	8	7.5	6.5	7	
Cold	R	11	10	11	10	9	
	Angle	36	39	34	33	38	36
Wet/used	H	6	6	5	5.5	5	
Warm	R	9	9	8	8	7	
	Angle	34	34	32	35	36	34

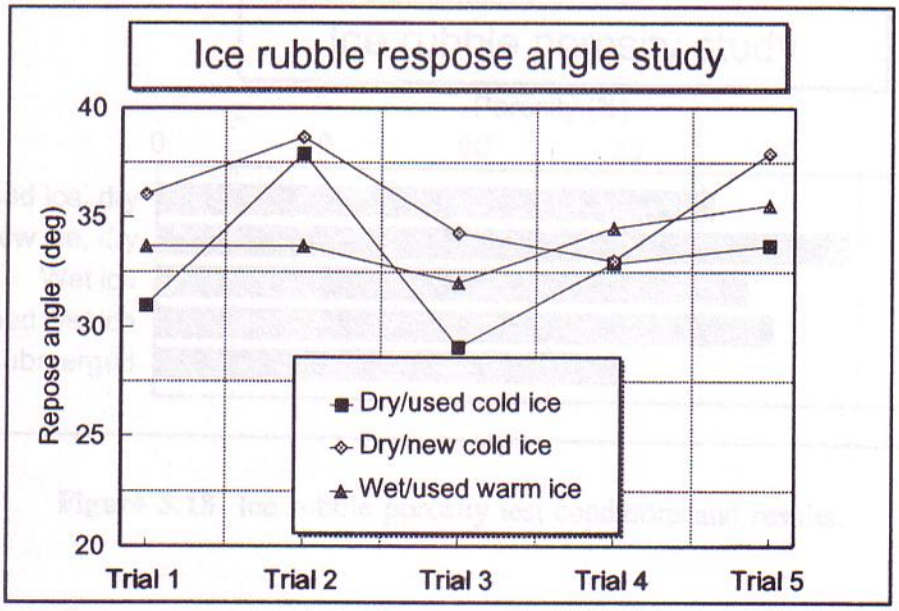

Figure 3.17 Ice rubble repose angle test conditions and results.

Test	Mass bucket Kg	Mass full bucket Kg	Mass water Kg	Volume water l	Porosity (%gas) %
Liquid water	1.78	21.09	19.31	19.31	0
Used ice, dry	1.78	12.94	11.16	12.40	36
New ice, dry	1.78	11.47	9.69	10.77	44
Wet ice	1.78	12.56	10.78	11.98	38
Drained wet ice	1.78	12.27	10.49	11.66	40
Submerged	1.10	15.70	14.60	16.22	29

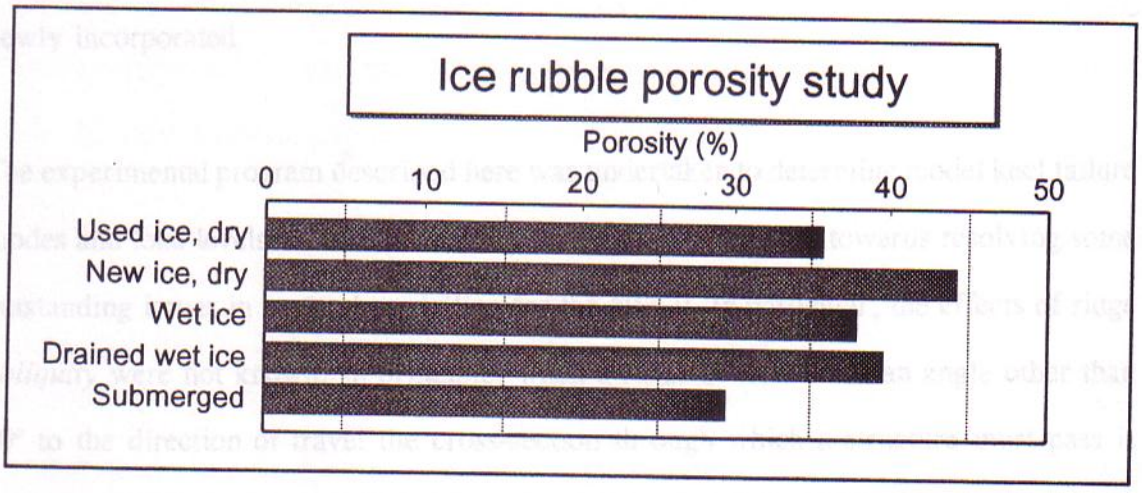

Figure 3.18 Ice rubble porosity test conditions and results.

3.2 Ridge failure at oblique approach angles[1]

3.2.1 Introduction

The physical laboratory tests with sand described in the previous section (and in Bruneau, 1994a) were extended so that some ridge failure patterns could be examined in more detail. They were motivated by the successful application of Section 3.1 results to the calibration of load prediction models for the Northumberland Strait Crossing Project. For example, the distinct local and plug-like failure modes observed justified the use of the *cross-over* modelling approach, and the consistent flaring of plug rupture planes was newly incorporated.

The experimental program described here was undertaken to determine model keel failure modes and load levels for certain loading conditions with a view towards resolving some outstanding issues in ice load modelling for the NSCP. In particular, the effects of ridge *obliquity* were not known. In principle, when a ridge is oriented at an angle other than 90° to the direction of travel the cross-section through which a structure must pass is extended. Seabed anchor pull-out experiments (reported by Vesic 1971, and others) indicated that rupture would strike out towards the nearest free surface and not follow the direction of travel. Otherwise, little guidance was found in the literature on the potential influence of oblique interactions on loads and rupture patterns. Experiments were undertaken to determine these obliquity effects and to investigate the influence of floor roughness and structure-to-keel size ratio on these effects.

---

[1] This study was sponsored by Public Works Canada at the request of K.R. Croasdale and Associates and reported as *Bruneau S.E. (1994b)* ***The indentation of sand formations.***

3.2.2 Scope of tests

The laboratory apparatus and testing procedures were similar to those in Subsection 3.1.3. Obliquity was expected to produce lateral loading on the structure so both longitudinal and lateral loads were measured. This was achieved by changing the support position of the uniaxial cantilever load cells. Experiments were repeated with opposite approach directions so that any bias in the axial measurement of "non-axial" loads would become evident.

Roughening the false floor was achieved by adhering sandpaper sheets (with grit size equivalent to sand particle size) to the entire floor area. The rough surface was intended to model the interlock expected between an ice ridge keel and the overlying refrozen core. Oblique "sand keels" were aligned according to painted angle markings on the floor.

3.2.4 Oblique ridge experimental results

Eight test series are reported in Table 3.1. The first four ("00", "10", "70", "80") refer to tests carried out on a smooth polyethylene floor inside the tank. The next two test series ("110", "120") were repeats of earlier ones, only they were performed on a roughened floor. The last two ("130" and "140") were performed on a rough floor and with a larger keel (depth H) and smaller structure (diameter D). These tests were aimed at determining the influence H/D on the obliquity force trends.

Figures 3.19 and 3.20 show plotted results and include schematics of the test series. Test series "10" and "70" are repeats of the default conditions with opposite approach directions. Similar results (for "00" and "80" also) confirmed that the data were

independent of the direction of loading on the cantilever load cells. For all the tests, the angle of obliquity was shown to increase longitudinal loads by a maximum of 20% though almost no effect was measured at angles below 50°. In fact, loads were sometimes reduced by as much as 10% at low oblique attack angles. Both longitudinal test series with the rough floor ("110" and "130") showed even less sensitivity to obliquity although it can been seen from Table 3.1 that roughening the floor increased structural loads by 10 to 25%. At a higher *H/D* ratio the influence of obliquity on longitudinal forces appeared to be diminished slightly at high obliquity angles but otherwise was similar to other test series.

Lateral loads ranged from almost zero for perpendicular entry to approximately half of the longitudinal force. Maximum lateral loads typically occurred at an oblique angle of 60°. The "exit force" (lateral force when structure leaves the "sand keel") often exceeded the "entry force" and was opposite in direction.

The modest influence of obliquity angle seen in these tests persuaded engineers to exclude it the design load strategy for the NSCP. The sensitivity of loads to the floor roughness was interpreted to suggest that, when modelling keel failure analytically, the internal friction angle of the rubble should be used as a friction coefficient on the horizontal shear plane.

Table 3.1 "Sand keel" obliquity experiments.

Test	Ridge obliquity deg	Keel width mm	Keel depth mm	Model diameter mm	Floor surface	Maximum force N	Minimum force N
						Lateral	Lateral
AN00	0	160	38	114	Smooth Poly.	0.558	-1.95
AN01	10	160	38	114	Smooth Poly.	0.639	-1.84
AN02	20	160	38	114	Smooth Poly.	0.607	-2.5
AN03	30	160	38	114	Smooth Poly.	0.853	-2.93
AN04	40	160	38	114	Smooth Poly.	1.03	-2.8
AN05	50	160	38	114	Smooth Poly.	1.35	-3.77
AN06	60	160	38	114	Smooth Poly.	1.49	-4.16
AN07	70	160	38	114	Smooth Poly.	1.71	-3.77
AN09	90	160	38	114	Smooth Poly.	0.51	-2.35
						Longitudinal	
AN10	0	160	38	114	Smooth Poly.	6.56	
AN11	10	160	38	114	Smooth Poly.	6.18	
AN12	20	160	38	114	Smooth Poly.	5.93	
AN13	30	160	38	114	Smooth Poly.	6.44	
AN14	40	160	38	114	Smooth Poly.	6.2	
AN15	50	160	38	114	Smooth Poly.	6.85	
AN16	60	160	38	114	Smooth Poly.	6.95	
AN17	70	160	38	114	Smooth Poly.	7.16	
AN18	90	160	38	114	Smooth Poly.	7.98	
						Longitudinal	
AN77	10	160	38	114	Smooth Poly.	6.54	
AN78	20	160	38	114	Smooth Poly.	6.56	
AN70B	30	160	38	114	Smooth Poly.	6.3	
AN71	40	160	38	114	Smooth Poly.	6.8	
AN72	50	160	38	114	Smooth Poly.	6.77	
AN73	60	160	38	114	Smooth Poly.	7.07	
AN74	60	160	38	114	Smooth Poly.	7.32	
AN75	70	160	38	114	Smooth Poly.	7.44	
AN76	90	160	38	114	Smooth Poly.	7.93	
						Lateral	Lateral
AN80	0	160	38	114	Smooth Poly.	2.26	-0.84
AN81	10	160	38	114	Smooth Poly.	2.25	-1.31
AN82	20	160	38	114	Smooth Poly.	2.45	-0.755
AN83	30	160	38	114	Smooth Poly.	3.05	-0.576
AN84	40	160	38	114	Smooth Poly.	3.8	-1.24
AN85	50	160	38	114	Smooth Poly.	3.97	-1.63
AN86	60	160	38	114	Smooth Poly.	4.08	-1.72
AN87	60	160	38	114	Smooth Poly.	4,23	-1.61
AN88	70	160	38	114	Smooth Poly.	4.49	-1.78
AN89	90	160	38	114	Smooth Poly.	2.85	-1.81
						Longitudinal	
AN113	0	160	38	114	Rough grit	8.27	
AN116	30	160	38	114	Rough grit	8.68	
AN114	60	160	38	114	Rough grit	8.42	
AN115	90	160	38	114	Rough grit	8.7	
						Lateral	Lateral
AN120	0	160	38	114	Rough grit	0.43	-2.3
AN121	30	160	38	114	Rough grit	0.64	-2.52
AN122	60	160	38	114	Rough grit	1.71	-4.07
AN123	90	160	38	114	Rough grit	0.95	-1.62
						Longitudinal	
AN130	0	320	76	60	Rough grit	23.17	
AN131	0	320	76	60	Rough grit	23.17	
AN132	30	320	76	60	Rough grit	22.02	
AN133	50	320	76	60	Rough grit	24.44	
AN134	90	320	76	60	Rough grit	22.15	
AN135	0	160	76	60	Rough grit	5.72	
						Lateral	Lateral
AN140	0	320	76	60	Rough grit	0.64	-3.17
AN141	30	320	76	60	Rough grit	1.44	-6.25
AN142	50	320	76	60	Rough grit	2.82	-7.64
AN143	90	320	76	60	Rough grit	0.4	-3.63

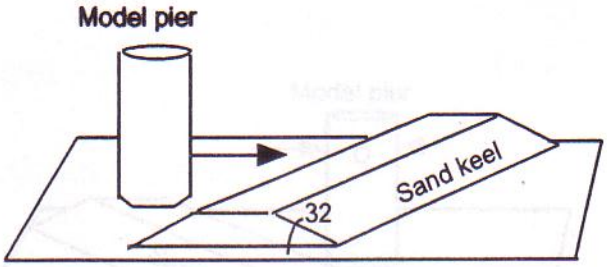

Isometric schematic

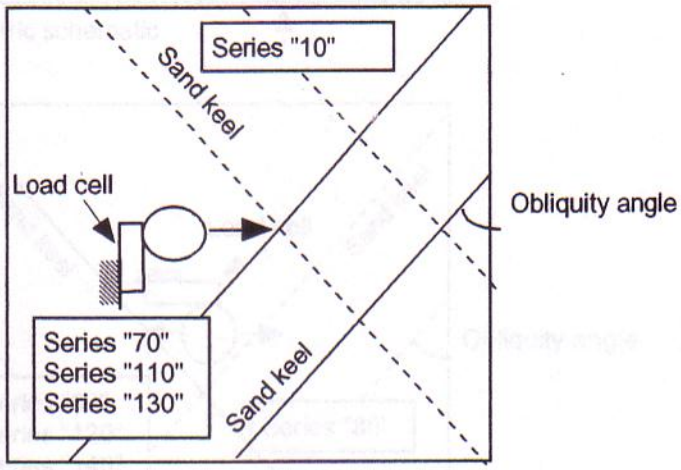

Plan schematic

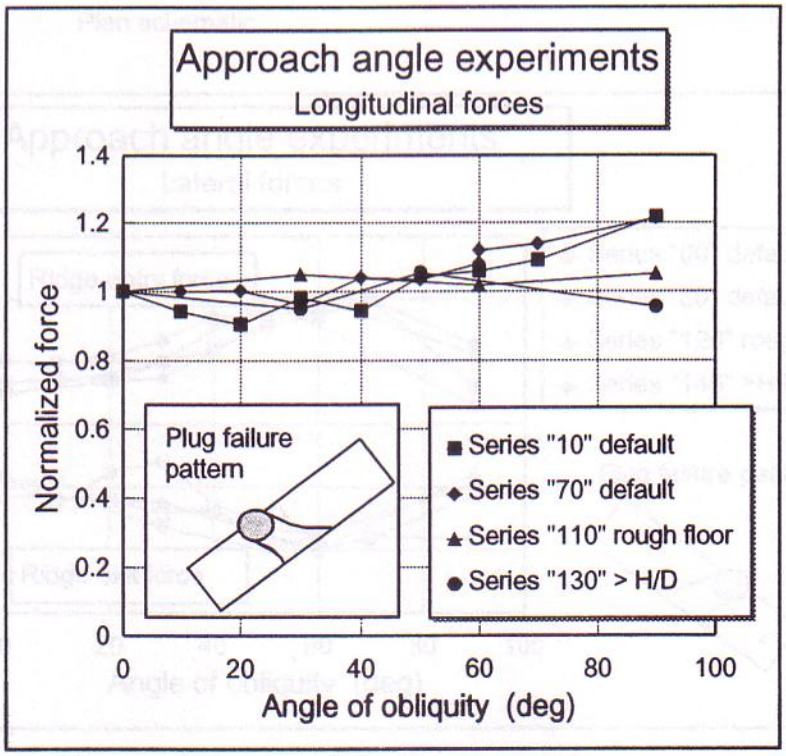

Figure 3.19 "Sand keel" longitudinal forces.

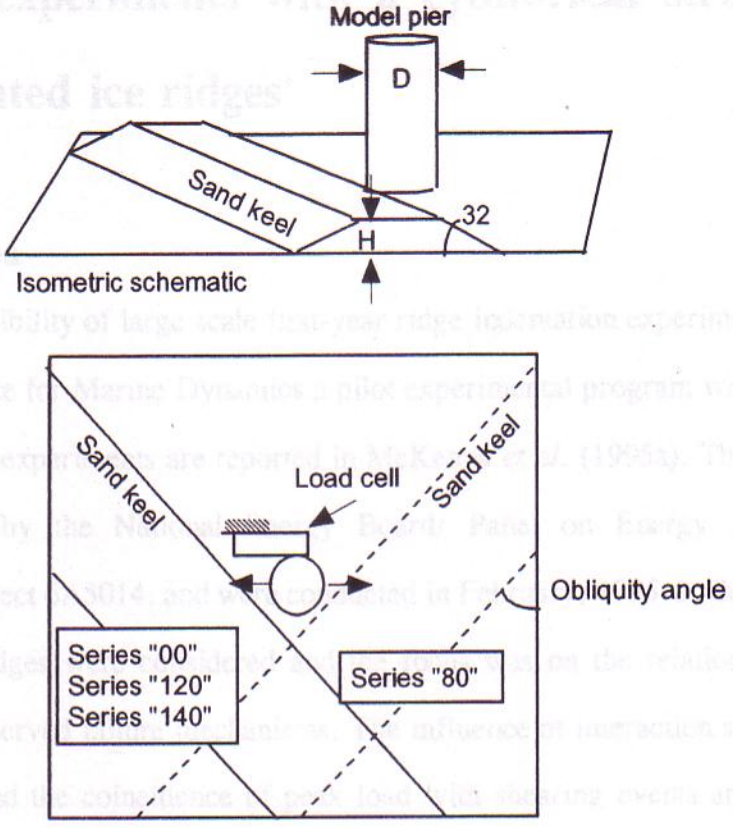

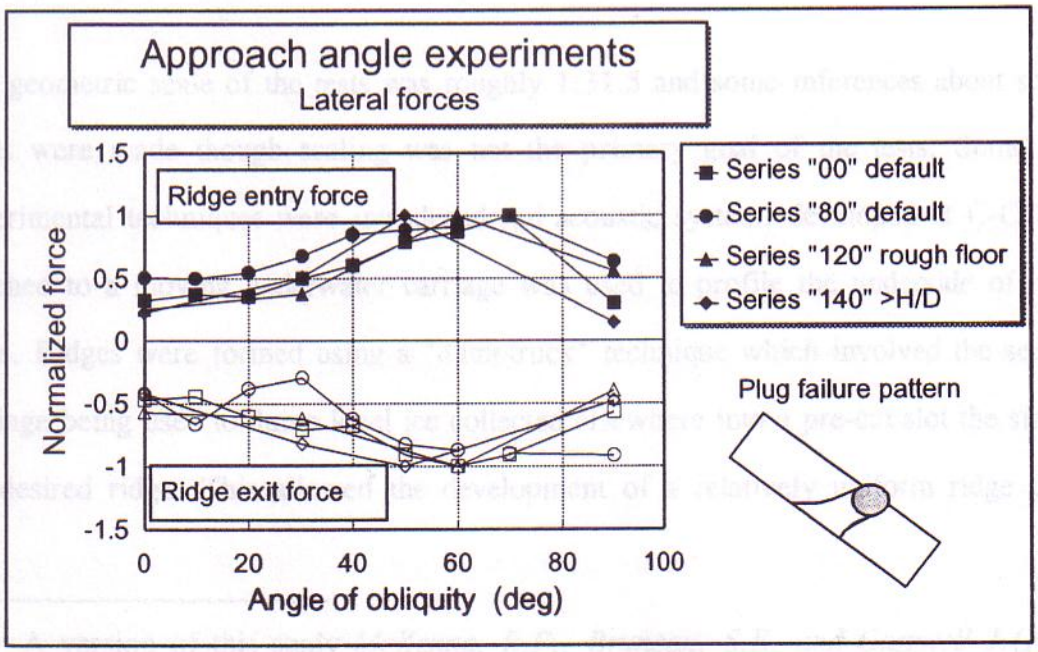

Figure 3.20 "Sand keel" lateral forces.

3.3 Pilot experiments with a cylindrical structure in unconsolidated ice ridges[1]

3.3.1 Introduction

To assess the feasibility of large scale first-year ridge indentation experiments in the ice tank at the Institute for Marine Dynamics a pilot experimental program was carried out. The details of the experiments are reported in McKenna *et al.* (1995a). The experiments were sponsored by the National Energy Board/ Panel on Energy Research and Development Project 6A5014, and were conducted in February, 1995. In the experiments unconsolidated ridges were considered and the focus was on the relation between the forces and the observed failure mechanisms. The influence of interaction speed was also given attention and the coincidence of peak load with shearing events and penetration distances was noted.

The geometric scale of the tests was roughly 1:31.5 and some inferences about scaled loads were made though scaling was not the primary goal of the tests. Some new experimental techniques were introduced: an acoustic system, developed at C-CORE, attached to a moving underwater carriage was used to profile the underside of ridge keels. Ridges were formed using a "dumptruck" technique which involved the service carriage being used to dump level ice collected elsewhere into a pre-cut slot the size of the desired ridge. This allowed the development of a relatively uniform ridge cross

[1] A version of this study *McKenna, R.F., Bruneau, S.E. and Guzzwell J.(1997)* ***Modelling unconsolidated rubble forces on a cylindrical structure*** has been prepared for POAC/OMAE 1997, Yokohama, Japan.

section across the 12 m wide tank. A digital video image processing technique to determine block size distribution and under and above water time-encoded video systems were used to document the tests.

3.3.2 Scope of experiments

The structure was a 0.32 m diameter aluminum cylinder. Two parallel ridges with a space of 3 m between were built from a 3 cm thick ice sheet. Ridges were not consolidated as tests commenced shortly after ridges were built at a room temperature of 2° C. The ice around the test area remained intact for the test period to provide support boundary conditions for the ridges during indentation. The first ridge, 2 m wide, was indented twice and the second, 3 m wide, was indented four times. Interaction speed was systematically varied over one order of magnitude. Video records of the interactions were obtained from two positions above and two beneath the water surface.

3.3.3 Experimental results

Results are summarized in Figure 3.21. Of the six tests all but the first failed in patterns characterized by local failure giving way to plug formation. Ridge failure in front of the structure for the first 20 to 40% of the width was characterized by a local repositioning of blocks with some above water surcharge developed but none below. Beyond this position a large wedge of intact rubble was mobilized up to the speed of the advancing structure. Before the structure exited the ridge the wedge was forced off to one side of the structure's path (without directional preference) and under the level ice layer. The first experiment, at the lowest speed, resulted in a global shift of the ridge as it failed in flexure and slid under the supporting ice layer to the rear.

As shown in Figure 3.21 longitudinal forces were insensitive to interaction speed over the range of test conditions. A non-linear increase in load with ridge sectional area was observed. Of particular interest was the close correspondence of incipient plug failure with maximum longitudinal loads. Lateral loads were, on average, 30% of longitudinal and lagged behind also so that resultant loads were only marginally greater than longitudinal. Remarkably, almost exactly the same loads were measured for the first two tests in which observed failure modes differed considerably. If further substantiated, this result could play an important role in future modelling efforts.

These experiments were of value for a number of reasons. The observed failure modes and associated load levels supported the accepted analytical modelling strategy for design loads on the Northumberland Strait Bridge. The acoustic profiler was successful in mapping the bottom profile of the ridge, and, the "dumptruck" ridge construction technique yielded a block size distribution that was strikingly similar to that which was measured in the field in Veitch *et al.* (1991a).

The robust procedure developed in this test series provided the groundwork for larger scale first-year ridge experiments to be undertaken at IMD.

	Run 1	Run 2	Run 3	Run 4	Run 5	Run 6
RIDGE PROPERTIES						
Ridge #	1	1	2	2	2	2
Ridge width (m)	2	2	3	3	3	3
Ridge sail x-section area (m^2)	0.1	0.1	0.15	0.15	0.15	0.15
Rridge keel x-section area (m^2)	0.59	0.59	1	1	1	1
Total ridge x-section area (m^2)	0.69	0.69	1.15	1.15	1.15	1.15
Block density (kg/m^3)	857	857	871	871	871	871
Ridge porosity	0.26	0.26	0.27	0.27	0.27	0.27
INTERACTION DATA						
Speed (m/s)	0.019	0.187	0.187	0.131	0.075	0.019
Ice/structure friction coef.	0.13	0.13	0.13	0.13	0.13	0.13
Structure diameter (m)	0.32	0.32	0.32	0.32	0.32	0.32
Logitudinal						
Peak longitudinal force (N)	332	331	852	592	692	541
Displacement to peak longit. (m)	0.342	0.595	1.336	1.177	1.05	0.681
Fraction of ridge to peak longit.	0.171	0.298	0.445	0.392	0.350	0.227
Lateral						
Peak lateral force (N)	68	73	121	177	171	347
Displacement to peak lat.. (m)	0.674	1.74	2.18	1.283	1.16	1.418
Fraction of ridge to peak lat.	0.337	0.870	0.727	0.428	0.387	0.473
Resultant						
Peak resultant force (N)	332	332	852	594	703	557
Displacement to peak res. (m)	0.342	0.595	1.336	1.203	1.05	1.272
Fraction of ridge to peak res.	0.171	0.298	0.445	0.401	0.350	0.424
VIDEO DATA						
Distance to plug (m)	0.38	0.81	1.17	1.1	1	0.64
Fraction of ridge to plug	0.19	0.41	0.39	0.37	0.33	0.21
Wedge flare angle (deg)	-	30	30	30	45	-
Max. wedge width (in diameters)	-	3 D	4 D	3-4 D	>5 D	
Surcharge height above water (cm)	13	12	20	21	21	12

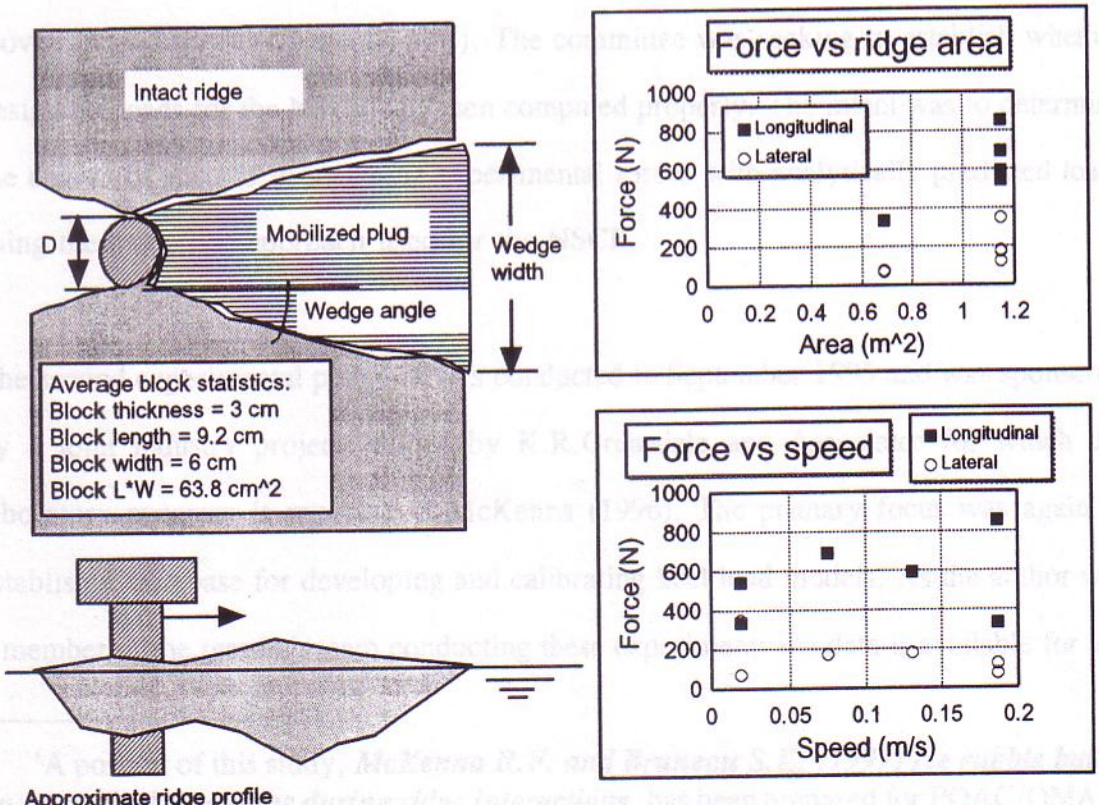

Figure 3.21 Test conditions and results - pilot experiments at IMD.

3.4 Large-scale ridge interaction experiments[1]

3.4.1 Introduction

Two sets of experiments, independently planned and sponsored but similarly executed, are described in this thesis section. Both programs utilized test procedures developed in McKenna *et al.* (1995a) and described in Section 3.3. The two programs represent the largest scale first-year ridge indentation laboratory experiments in the literature (though proprietary). The first program was conducted to address the interaction between a model pier from the Northumberland Strait Crossing Project and first-year ridges (McKenna *et al.* 1995b). Experiments were conducted at the Institute for Marine Dynamics in June 1995. The tests were requested by the Ice Interaction Subcommittee for the Northumberland Strait Crossing Project and were sponsored by Public Works and Government Services Canada (PWC). The committee was seeking to establish whether design ice loads for the NSCP had been computed properly. The intent was to determine the degree of success in matching experimental forces with analytically predicted loads using the modelling approach used for the NSCP.

The second experimental program was conducted in September 1995 and was sponsored by a joint industry project headed by K.R.Croasdale and Associates for which the laboratory program is reported in McKenna (1996). The primary focus was again to establish a data base for developing and calibrating keel load models. As the author was a member of the research team conducting these experiments the data is available for use

---

[1]A portion of this study, ***McKenna R.F. and Bruneau S.E. (1997) Ice rubble build-up on conical structures during ridge interactions***, has been prepared for POAC/OMAE, 1997, Yokahama, Japan.

in this thesis (though it remains proprietary).

3.4.2 Scope of experiments

The model pier used in both experimental programs was comprised of a conical ice shield at the waterline and a cylindrical shaft below (see the figure in Table 3.2). The shaft diameter was 0.8 m and the cone was 1.825 m at the base and had an angle of 45°. The cone and the cylinder were instrumented separately. In total, twenty-nine experiments were performed on fifteen ridges most of which were constructed from an entire ice sheet using the "dumptruck" technique. The focus of the test program was on the forces exerted on the structure by the rubble in the ridge keels. Most ridges were refrozen to form a thin consolidated core at the waterline which provided a realistic boundary condition for the keel. The cone lifted the core and sheet ice so that ice crushing was avoided, preserving the structural configuration and function of the NSCP bridge piers. The test parameters were water level, speed, rubble strength, ridge shape, ridge orientation and structure diameter. In the second test program a few experiments were conducted with the lower cylinder replaced by a large one (1.8 m diameter) and with no consolidated core present.

In an attempt to ascertain the shear strength of ice rubble in the ridge keels at IMD a "punch" shear technique was developed. The tests were similar to subsea plate anchor pull-out experiments except that they were inverted (push down) and the refrozen core needed to be presawn. Details of the experiments, the analysis technique and results are found in McKenna R., Bruneau S. and Williams, M. (1996). In Table 3.2 the shear strength of the ice rubble is shown to remain constant for all tests. It is quite possible that the rubble shear strength varied from test to test, however, there was considerable

scatter in the punch shear data set. Without a consensus amongst the research team on how to interpret the data, only the approximate mean value for unconsolidated keel rubble strength has been quoted.

3.4.3 Experimental results

Details of the test conditions and results are found in McKenna *et al.* (1995b) and McKenna (1996) (referred to as the PWC and JIP tests respectively). Table 3.2 lists most key test conditions and results. With so many test variables, some of which may be correlated, it is difficult to conclusively isolate singular effects. Nevertheless, some general trends are exposed in the figures which accompany the table. They show that keel forces on the cylinder are strongly influenced by keel depth and structural diameter, are influenced much less by apparent block flexural strength and are quite insensitive to ridge width and approach speed. Also from the table one can deduce that ridge keel shape and structure roughness are not key control parameters. Peak cylinder and cone forces were not simultaneous and the peak resultant was on average 5.8% less than the sum of the two. However, it cannot be readily concluded that the core and keel will not fail simultaneously in the field since lab ridges were not heavily consolidated and tended to be double-keeled with the sail arched between (probably an artifact of the "dumptruck" building technique).

Forces on the cone were not the focus of these experiments. However, the data set provides a unique opportunity for development and testing of models for rubble forces on conical structures. The topic is discussed later in this thesis.

Table 3.2 Large-scale test conditions and results.

Test program		PWC	PWC	PWC	PWC	PWC	PWC	PWC	PWC	PWC	PWC	PWC
Ice sheet		1	1	2	2	3	3	4	4	5	6	6
Run		1	2	1	2	1	2	1	2	1	1	2
Cylinder diameter	m	0.8	0.8	0.8	0.8	0.8	0.8	0.8	0.8	0.8	0.8	0.8
Cylinder surface		smooth	smooth	smooth	smooth	smooth	smooth	smooth	smooth	smooth	smooth	smooth
Cone base diameter	m	1.825	1.825	1.825	1.825	1.825	1.825	1.825	1.825	1.825	1.825	1.825
Cone angle		45	45	45	45	45	45	45	45	45	45	45
Speed	m/s	0.424	0.141	0.141	0.141	0.141	0.0283	0.141	0.141	0.141	0.141	0.141
Water level to cone base	m	0.08	0.08	0.08	0.32	0.08	0.08	0.08	0.32	0.08	0.08	0.32
Ridge orientation		90	90	90	90	90	90	90	90	45	90	90
Keel width	m	4.5	4.5	4.9	4.9	6	6	6	6	4.6	4.5	4.5
Max keel depth	m	1.1	1.1	1.1	1.1	1.1	1.1	0.9	0.9	1.05	1.1	1.1
Keel depth below cone	m	1.02	1.02	1.02	0.78	1.02	1.02	0.82	0.58	0.97	1.02	0.78
Max sail height	m	0.24	0.24	0.17	0.17	0.18	0.18	0.25	0.25	0.22	0.21	0.21
Av keel x-section area	m^2	3.8	3.8	4.24	4.24	3.52	3.52	3.36	3.36	3.41	3.77	3.77
Av sail x-section area	m^2	0.4	0.4	0.41	0.41	0.47	0.47	0.47	0.47	0.38	0.39	0.39
Keel block density	kg.m^3	931	931	933	933	923	923	926	926	931	932	932
Sail block density	kg.m^3	905	905	917	917	906	906	900	900	905	911	911
Porosity		0.32	0.32	0.4	0.4	0.3	0.3	0.27	0.27	0.32	0.35	0.35
Block thickness	mm	50.9	50.9	50.4	50.4	49.5	49.5	50.5	50.5	50	47.2	47.2
Level ice thickness	mm	59.3	59.3	59.3	59.3	59	59	59.6	59.6	59.4	58.6	58.6
Consolidated layer thickness	mm	58.3	58.3	20	20	53.3	53.3				40	40
Level ice flex, initial	kPa	32.5	32.5	34.5	34.5	35.5	35.5	37.5	37.5	36.5	73	73
Level ice flex strength at test	kPa	60.5	60.5	82	82	81.75	81.75	69.5	69.5	74.5	82	82
Block flex strength	kPa	27.5	27.5	20.5	20.5	25.5	25.5	19.5	19.5	15.5	32	32
Consol. core flex strength	kPa	74.5	74.5			81.3	81.3					
Friction angle		36	36	36	36	36	36	36	36	36	36	36
Cohesion	pa	438	438	438	438	438	438	438	438	438	438	438
Cylinder peak X force	N	3110	2650	2170	1080	2760	3110	2440	870	2810	3950	1560
Cone peak X force	N	3370	3060	2790	5520	3010	2930	3160	5300	3340	3650	7070
Total peak X force	N	6130	5350	4670	6290	5720	5940	5300	5980	5530	7110	8330
Cylinder peak Y force (port)	N	290	320	340	560	370	570	330	400	1020	360	740
Cylinder peak Y force (starb.)	N	330	370	410	60	400	140	150	160	830	490	180
Cone peak Y force (port)	N	470	300	500	1450	650	550	450	1660	910	340	1710
Cone peak Y force (starb.)	N	400	680	240	50	290	190	270	150	450	470	10
Total peak Y force (port)	N	670	470	580	1920	700	790	520	1860	1820	490	2100
Total peak Y force (starb.)	N	530	850	530	60	390	120	320	160	890	660	0
Total Z force	N	2980	2610	2840	3940	2440	1760	2390	3780	2280	2530	4850
Penet at peak cyl. X force	m	3.1	2.9	3.1	3.0	3.5	3.3	2.9	2.7	3.6	2.6	2.6
Penet at peak cone. X force	m	2.6	2.4	2.5	2.5	3.2	3.2	2.8	3.1	3.2	2.3	2.2
Penet at peak tot. X force	m	3.1	2.9	3.1	2.5	3.2	3.2	2.8	3.1	3.6	2.6	2.2
Penet at peak Z force	m	3.9	3.9	3.5	3.9	3.7	5.2	4.6	4.7	4.6	2.9	2.1

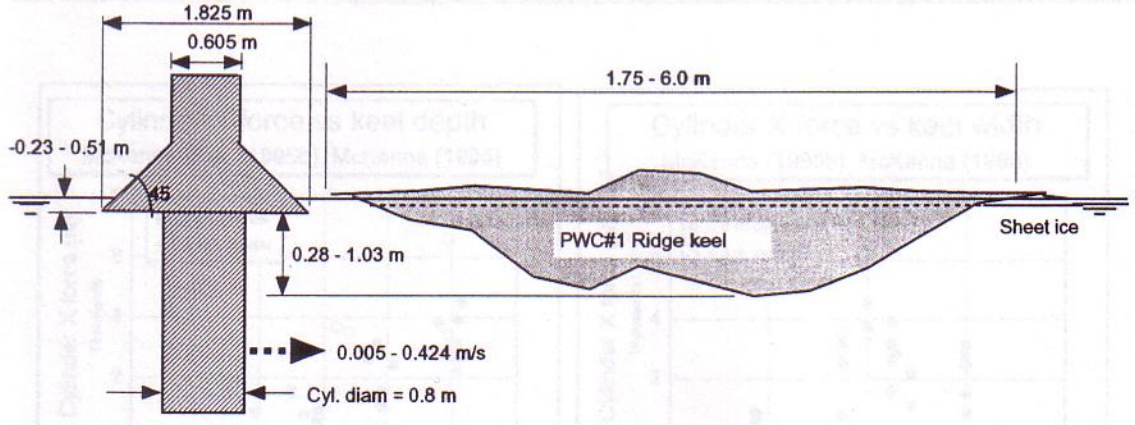

Table 3.2 (continued).

Test program		JIP	JIP	JIP	JIP	JIP	JIP	JIP	JIP	JIP	JIP	JIP
Ice sheet		4	4	5	5	6	6	7	7	7	7	8
Run		1	2	1	2	1	2	1	2	3	4	1
Cylinder diameter	m	0.8	0.8	0.8	0.8	0.8	0.8	0.8	0.8	0.8	0.8	1.8
Cylinder surface		smooth	smooth	rough	smooth	smooth	smooth	smooth	smooth	smooth	smooth	smooth
Cone base diameter	m	1.825	1.825	1.825	1.825	1.825	1.825	1.825	1.825	1.825	1.825	1.825
Cone angle		45	45	45	45	45	45	45	45	45	45	45
Speed	m/s	0.07	0.07	0.07	0.07	0.07	0.07	0.07	0.005	0.005	0.07	0.07
Water level to cone base	m	0.32	0.08	0.08	0.08	-0.23	0.51	0.08	0.08	0.08	0.08	0.08
Ridge orientation		90	90	90	90	90	90	90	90	90	90	90
Keel width	m	3.5	3.5	4	4	6	6	3.5	3.5	1.75	1.75	3.5
Max keel depth	m	0.86	0.82	1.11	1.04	0.5	0.59	1.09	0.85	0.47	0.66	0.76
Keel depth below cone	m	0.54	0.74	1.03	0.96	0.5	0.08	1.01	0.77	0.39	0.58	0.68
Max sail height	m	0.12	0.14	0.23	0.25	0.06	0.08	0.2	0.2	0.16	0.07	0.23
Av keel x-section area	m^2	2.495	2.34	2.693	2.693	3.097	3.107	2.378	2.079	0.595	0.761	1.59
Av sail x-section area	m^2	0.26	0.302	1	0.559	0.338	0.38	0.303	0.339	0.125	0.089	0.349
Keel block density	kg.m^3	903	903	895	895	895	895	906	906	906	906	913
Sail block density	kg.m^3	787	787	746	746	755	755	768	768	768	768	792
Porosity		0.27	0.27	0	0.16	0.23	0.23	0.18	0.18	0.28	0.28	0.05
Block thickness	mm	46.8	46.8	50.9	50.9	51.5	51.5	50.1	50.1	50.1	50.1	47.1
Level ice thickness	mm	56	56	56.2	56.2	51.5	51.5	56.4	56.4	56.4	56.4	55.3
Consolidated layer thickness	mm					0	0					
Level ice flex when ridge buil	kPa	55.5	55.5	59.5	59.5	61.5	61.5	64	64	64	64	66.5
Level ice flex strength at test	kPa			99	99	25	25	80	80	80	80	166.5
Block flex strength	kPa	37.5	37.5	44	44	31.5	31.5	24.5	24.5	24.5	24.5	21.5
Consol. core flex strength	kPa			81	81	74	74	244.5	244.5	244.5	244.5	254.5
Friction angle		36	36	36	36	36	36	36	36	36	36	36
Cohesion	pa	438	438	438	438	438	438	438	438	438	438	438
Cylinder peak X force	N	790	2610	4530	3770	1540		2540	3120	860	610	3520
Cone peak X force	N	5290	3780	3190	3290		2600	2840	3230	1910	2010	2810
Total peak X force	N	5910	6030	6610	6850	1510	2610	5290	5850	2600	2470	6030
Cylinder peak Y force (port)	N	170	720	240	1190	180		130	1060	160	50	390
Cylinder peak Y force (starb.)	N	180	120	460	70	590		440	40	30	60	270
Cone peak Y force (port)	N	360	860	460	780		1090	470	900	300	350	680
Cone peak Y force (starb.)	N	1050	280	340	130		10	320	310	250	370	300
Total peak Y force (port)	N	450	1420	620	1910	190	1090	360	1800	390	370	990
Total peak Y force (starb.)	N	1130	280	490	150	580	10	620	190	250	420	480
Total Z force	N	5080	2160	3320	2340		2460	2140	1680	1450	1770	2930
Penet at peak cyl. X force	m	2.3	1.7	2.2	2.4	2.7		1.6	1.8	0.8	0.5	2.0
Penet at peak cone. X force	m	2.2	2.4	4.1	3.0		4.8	1.9	2.0	0.9	1.1	1.5
Penet at peak tot. X force	m	2.2	2.4	2.6	3.0	2.7	4.8	2.0	2.2	1.2	1.1	1.9
Penet at peak Z force	m	2.2	2.5	4.1	4.3	6.2	5.3	3.1	4.1	2.1	1.3	2.3

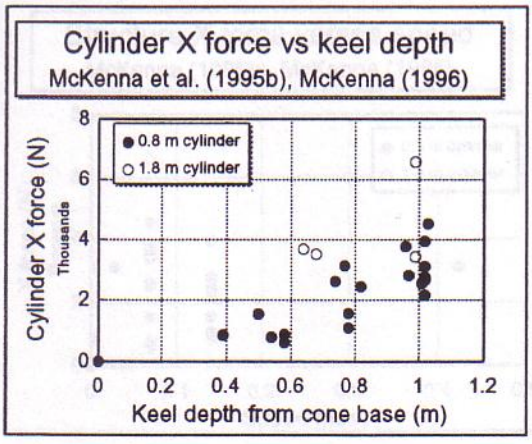

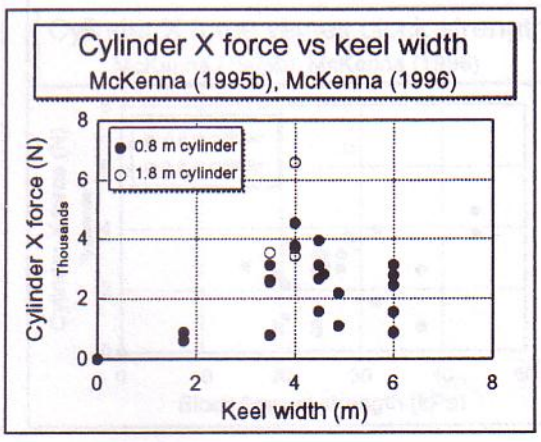

Table 3.2 (continued).

Test program		JIP	JIP	JIP	JIP	JIP	JIP	JIP
Ice sheet		8	8	8	9	9	10	10
Run		2	3	4	1	2	1	2
Cylinder diameter	m	1.8	1.8	1.8	1.8	1.8	1.8	1.8
Cylinder surface		smooth	smooth	smooth	smooth	smooth	smooth	smooth
Cone base diameter	m	1.825	1.825	1.825	1.825	1.825	1.825	1.825
Cone angle		45	45	45	45	45	45	45
Speed	m/s	0.07	0.07	0.07	0.07	0.07	0.07	0.07
Water level to cone base	m	0.32	0.32	0.08	-0.23	-0.23	0.32	0.08
Ridge orientation		90	90	90	90	90	90	90
Keel width	m	3.5	1.75	1.75	4	4	4	4
Max keel depth	m	0.75	0.56	0.37	0.99	0.95	0.96	1.07
Keel depth below cone	m	0.43	0.24	0.29	0.99	0.95	0.64	0.99
Max sail height	m	0.23	0.11	0.15	0.27	0.21	0.26	0.22
Av keel x-section area	m^2	1.811	0.642	0.502	2.884	2.906	2.905	3.428
Av sail x-section area	m^2	0.372	0.12	0.091	0.479	0.503	0.489	0.472
Keel block density	kg.m^3	913	913	913	894	894	902	902
Sail block density	kg.m^3	792	792	792	743	743	751	751
Porosity		0.05	0.21	0.21	0.18	0.18	0.24	0.24
Block thickness	mm	47.1	47.1	47.1	49.8	49.8	50	50
Level ice thickness	mm	55.3	55.3	55.3	49.8	49.8	59.2	59.2
Consolidated layer thickness	mm				0	0	36	36
Level ice flex when ridge buil	kPa	66.5	66.5	66.5	60.5	60.5	43	43
Level ice flex strength at test	kPa	166.5	166.5	166.5	16	16	107	107
Block flex strength	kPa	21.5	21.5	21.5	29.5	29.5	28.5	28.5
Consol. core flex strength	kPa	254.5	254.5	254.5	116.5	116.5	232.5	232.5
Friction angle		36	36	36	36	36	36	36
Cohesion	pa	438	438	438	438	438	438	438
Cylinder peak X force	N				3420		3690	6580
Cone peak X force	N						6030	3110
Total peak X force	N	6510	3100	2690	3730	2460	9270	8890
Cylinder peak Y force (port)	N				1670		1110	1710
Cylinder peak Y force (starb.)	N				340		350	340
Cone peak Y force (port)	N						820	830
Cone peak Y force (starb.)	N						210	250
Total peak Y force (port)	N	2580	560	510	2050	60	1490	2540
Total peak Y force (starb.)	N	120	270	260	390	760	340	260
Total Z force	N	4780	3140	2000	340	10	6570	3510
Penet at peak cyl. X force	m				0.2		2.2	2.1
Penet at peak cone. X force	m						3.0	1.8
Penet at peak tot. X force	m	2.0	1.2	1.3	0.2	1.2	1.9	1.8
Penet at peak Z force	m	2.0	1.3	1.8			3.0	3.1

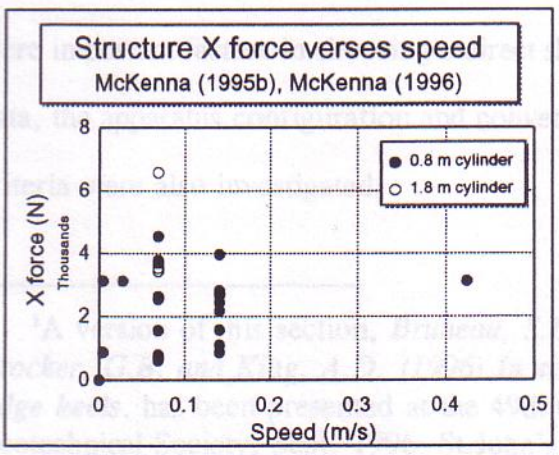

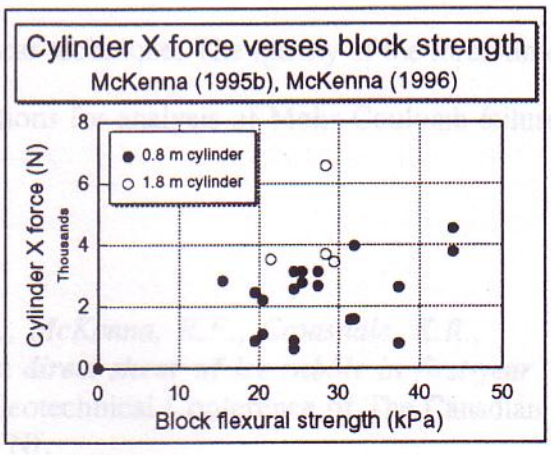

3.5 *In situ* direct shear of ridge keels[1]

3.5.1 Introduction

In this section a technique for direct *in situ* field measurement of rubble shear strength which has been developed and tested in the laboratory is described. The study was prompted by the requirement for accurate full-scale ice rubble properties for predicting ridge loads on structures. The technique involves lowering a ram and associated apparatus into a precut slot in a pressure ridge. This facilitates direct horizontal shear measurements of undisturbed keel ice rubble.

The experiments were conducted in the ice tank at the Institute for Marine Dynamics and were sponsored by the National Energy Board and administered by K.R. Croasdale and Associates. Model ice was used to build partially refrozen ridges, which were then sheared along a horizontal plane just below the consolidated layer using three different direct shear techniques. The apparatus, a scaled model of that proposed for field use, was designed after a rigorous evaluation of the suitability of various types of both direct and indexed shear tests (Croasdale *et al.*, 1996). The robustness of direct shear methods and the unambiguous analysis required to obtain estimates of cohesion and internal friction were important factors in choosing a direct shear technique. The quality of the force-time data, the apparatus configuration and conventions for analysis of Mohr-Coulomb failure criteria were also investigated.

---

[1]A version of this section, *Bruneau, S.E., McKenna, R.F., Croasdale, K.R., Crocker, G.B. and King, A.D. (1996)* ***In situ direct shear of ice rubble in first-year ridge keels***, has been presented at the 49th Geotechnical Conference of The Canadian Geotechnical Society, Sept. 1996, St.John's, Nf.

3.5.2 Test conditions

Experimental setup and model ice ridges

The tests were conducted on two ice ridges with parent ice sheet thicknesses of 30 mm and 50 mm. Since the constituent block thickness of ridges in temperate regions is of the order of 0.2 m to 0.5 m, scales ranging from 1:4 to 1:17 were modelled.

EG/AD/S model ice was used to build the ridges. Density and flexural strength were measured at the time of ridge formation and at test time. Fine bubbles were introduced during the freezing process to achieve a realistic density which was 895 kg/m^3 for keel blocks and 750 kg/m^3 for the sail blocks. The flexural strength measured in the level ice varied from 32 kPa to 62 kPa during ridge construction. At test time, keel samples yielded flexural strengths of the order of 30 kPa while sail ice samples ranged from 134 to 266 kPa. The full-scale flexural strength of sea ice ranges from below 300 kPa to 700 kPa.

The ridges were constructed for the present test program using the "dumptruck" technique as briefly described in Section 3.3. In this study a channel 4 m wide, spanning the entire 12 m width of the tank was cut in the level ice and fifty-five metres of level ice from elsewhere in the tank were lifted using the service carriage and dumped into the channel. The ice broke into pieces during placement since repeated drops were made at the centre of the channel. The ridges were supported on the front edge by the adjacent level ice sheet and on the back by a floating dock spanning the width of the tank as shown in Figure 3.22. A cooling cycle following the ridge construction created a refrozen layer within each ridge at the waterline.

Shear box apparatus

The rectangular shear box was constructed of welded aluminum plate with nominal dimensions of 0.75m long x 0.5m wide x 0.4m deep. The box consisted of upper and lower halves of equal depth connected by a slotted runner bearing positioned on overlapping flanges. The shearing action was achieved by relative motion of the two halves. The length of the bottom half of the box was 0.85m to allow the insertion of a spreader device. The assembly is shown in Figure 3.23.

The spreader was a self-contained assembly consisting of a hydraulic ram mounted rigidly to an aluminum plate. Four parallel guide rods were fixed to another plate which slid through holes in the first plate. A button load cell was placed on the end of the piston and a displacement potentiometer ("yoyo" type) was positioned between the spreader plates. The whole unit was easily detachable from the shear box so it could be incorporated into all direct shear options without disturbance of the data acquisition and drive systems.

For a typical sandy soil, laboratory shear devices split the sample across thousands of grains leading to uniform shearing which is representative of continuum behaviour. Ice rubble is, by contrast, a granular material with particles that are orders of magnitude larger. The size of the shear plane which would allow for similar particle kinematics and shear surface uniformity would prohibit direct scaling of soils shear devices. Thus, a consideration of the particle orientation, size and dynamics in a shear box is necessary to adequately model continuum behaviour. These considerations were reviewed as a part of this thesis and it was found that the average ratio of shear plane width to ice block length for 19 ice rubble shear tests in the literature was 6.4. The experiments with the

smallest shear box size-to-block ratios were conducted by Prodanovic (1979) who demonstrated that shear strength was unchanged when the block size was reduced from one half to one quarter of the width of the box. Furthermore, the results were repeatable and have been shown to be representative of results reported more recently. A box width of 0.5 m was chosen giving a box-to-block size ratio of 5.5 for 30 mm ice and 3.3 for 50 mm ice.

The elevation of the horizontal shear plane was selected such that shearing would be initiated below the refrozen core and beyond the reach of blocks frozen into it. As well, the elevation was maintained close to the undersurface of the refrozen layer to minimize the box depth and trenching requirements. Although the shear box could be lowered to any depth within the ridge, it was designed so that it could be conveniently and repetitively placed in the ridges with the shear plane positioned 10 cm below the lower surface of the refrozen layer.

Shear box options 1, 2 and 3

Three direct shear options were considered in the laboratory. In all three cases the apparatus was placed in a pre-cut trench in the ridge. Option 1 involved the use of the entire shear box assembly. Option 2 involved the removal of the lower half of the box and the placement of a reaction plate on the spreader assembly. The objective of this option was to provide a frame that would contain the *in situ* rubble sample and to guide the shear plane along the bottom edge of the box. In this case the shear plane reaction force was carried by the refrozen layer adjacent to the spreader. The absence of the lower half of the shear box reduced the depth of the rubble to be trenched and decreased the size and weight of the apparatus.

Option 3 eliminated the box altogether and relied upon the refrozen core to keep the *in situ* sample intact. Using only the spreader device, option 3 was implemented in three different configurations. In the first arrangement, 500 mm x 350 mm plates were attached to both spreader plates to allow for a larger bearing surface on the ice. In the second, the extra plate bearing against the *in situ* sample was removed and the spreader was moved down to bear directly against the refrozen layer. In the third, the guide rods were removed eliminating all possible sources of apparatus friction. Figure 3.24 is a schematic representation of the experiments showing the site before, and after, the placement of the apparatus for options 1 and 3.

Test plan and procedure

Two ice sheets were used in the test program. The first ridge was built from level ice 30 mm thick and the consolidated layer depth was approximately 40 mm. The second ridge was built from a 50 mm thick sheet and had the same consolidated layer depth. Both ridges were tempered so that the air temperature during testing was near the freezing point.

Before trenching, the ridge sail was levelled to a surface approximately 10 cm above the water level. To aid with the trenching, a template matching the shape of the interior of the shear box was placed over the ridge sail. The pattern was then vertically sawn through the sail core and keel to a predetermined depth below the core around 200 mm. At one end of the trench rectangular sections of the sail core and keel were removed by hand for placement of the spreader unit. At the opposite end of the trench, blocks were removed to allow free translation of the sheared sample.

The shear box was lowered over the undisturbed rubble by hand and keel depth, sail height and box position were measured. To increase vertical stresses in the undisturbed sample, fixed weights were distributed evenly on a plywood board placed on the levelled surface of the sail. Surcharges of approximately 500 Pa and 1000 Pa were achieved by using fixed weights of 20 kg and 40 kg. All tests were conducted at a shear rate of 2.1 cm/s.

Following the complete set of shear experiments on the first ridge (30 mm ice) it was decided that option 2 would be dropped from the second set of tests. As well, options 1 and 3 would be implemented without the spreader guide rods in place (hereafter referred to options 1a and 3a). It was apparent from the tests with the first ridge that the rods were the cause of enhanced friction and binding and did little to orient the spreader plates. Dry runs conducted prior to the second set of tests indicated a significant reduction in no-load box friction for option 1 without the guide rods. By removing the rods, peak friction was reduced by more than half the original 'with-rods' option. For option 3, removal of the guide rods meant that there was no frictional component to the load trace due to the apparatus.

3.5.3 Laboratory results

Ridge geometry

A ridge profile was measured by pushing a graduated aluminum rod through the keel. A length scale was used to measure the height of the sail relative to the service carriage platform. The measured profile for ridge 2 is shown in Figure 3.22.

Block dimensions resulting from the "dumptruck" ridge construction technique were estimated from video images of the floating rubble in a previous study where the same technique was used (McKenna *et al.*, 1995a). In that study, the block length and width dimensions in the plane of the water surface were determined for 160 blocks in a digitized video frame. The means of the length and width were 3.1 and 2.0 times the ice thickness. The smallest block widths were approximately equal to the level ice thickness. The largest block length was between 8 and 9 times the ice thickness. On average, the ratio of the length to the width was 1.6. These statistics are believed to be representative of those for this study since parent ice sheet properties were similar.

Force time series

Figure 3.25 shows force and displacement time series traces, two for option 1a and two for option 3a. Several "dry" runs were conducted to determine the no-load static and dynamic friction characteristics of the shear box. Averaged load traces of the frictional force for each shear option have been subtracted from the force traces and for all subsequent analyses.

Virtually all load traces exhibited a significant oscillatory component. Some fluctuations were more random than others but most were uniform and saw-toothed. During the tests, it was often possible to observe the "skipping" or hopping of the rubble sample corresponding to these load cycles. The frequency was observed to drop with decreasing normal stress, though the relation was not very strong. Option 3 produced both the highest (for original "with guide rods" option) and lowest (without rods) frequencies - apparently an artifact of the spreader mechanics. Oscillation amplitudes were observed to be poorly correlated to normal stress, although a slight trend towards increased

amplitude with apparatus "weight" was noted.

The potential causes of the force oscillations included ice-structure ratchetting, shear box stick-slip action, and ice rubble cyclic dilation. The author believes that the most likely cause was ratchetting in which, periodically, quasi-static forces on an ice-structure interface increase with increased deflection until ice resistance is exceeded, causing ice failure and a relief of loads on the structure. In this case, the appropriate measured force values to use in the interpretation are the peak values since this mechanism is not resonant and will not result in any dynamic amplification of the peak forces.

For options 1 and 2, the peaks of load cycles frequently grew with increased shear box translation. At appreciable box translations there was an increased normal stress due to the decrease in shear area, and the sample tilted into the trench. This may have led to enhanced compression and gouging at the leading and trailing box edges, complicating the analysis for options 1 and 2. Only option 3 (no shear box at all) exhibited a clear tendency for peak loads to repeatedly occur in the first few seconds.

Rubble shear stress

Analysis of the experimental data revealed that subjective decisions were required in order to determine shear strength, even for the least ambiguous of test procedures. Shear stress is often computed by dividing the force required to shear the sample by the instantaneous shear plane area of the box. Difficulty is encountered when forces are cyclic and peaks increase with displacement. The choice must then be made of when, or at what displacement, peak "shear resistance" was encountered. Loads which follow may be greater but may also be artifacts of the shear box mechanics. Furthermore, one may

wish to consider either peak or residual (mobilized) friction angles and, of these, either absolute maxima or mean cyclic values may be selected.

In this study two conventions were adopted. The first was to determine the peak shearing force from the first two seconds or 4.2 cm displacement. The second looked at the first 15 seconds or 30 cm of the force-time histories for a peak. The latter was selected to correspond to some observed trends in the force traces whereas the first was based on the assumption that for typical dilatant soils, shearing peak loads occur at displacements close to but less than one particle thickness. Shear areas were adjusted for box displacement.

Mohr-Coulomb approximation

Normal (vertical) shear plane stresses were determined from the weight of the ice above the surface, the buoyant weight of ice between the surface and the shear plane below and the weights added for surcharge. A plot of the results for the 2-second peak shear for all options is given in Figure 3.26 and for the 15-second peak shear in Figure 3.27. It is evident by comparing Figures 3.26 and 3.27 that using the 2 s instead of the 15 s adjusted shear strength values is probably justified. Increased scatter in the latter underscores the uncertainty about apparatus performance and shear interpretation beyond the first few seconds of each test. The uniform spread of the results for all apparatus options, and the close agreement between options indicates that the 2 s peak is analytically superior. An interesting result is obtained when both the combined 2 s and combined 15 s results are compared. Figure 3.28 shows that the internal friction angle for both was a near perfect match while apparent cohesion was 2/3 higher for the latter case.

Case (1991) reports laboratory results from the ice tank at IMD when a fixed vertical direct shear box was used to shear rubble samples. The ice rubble (similar to that in this study) was formed by a chopping action of the carriage and samples were corralled into the box. The shear rate was twenty times slower than that in the present tests and the timing of tests relative to ice formation was somewhat different. In spite of these differences, the laboratory results are similar. The results for the Case (1991) study for all tests combined were $\phi = 38°$ and c = 661 Pa whereas the combined results in the present study are $\phi = 41°$ and c = 873 Pa. This is a strong indication that the direct shear approach is robust and that the influence of block size and test conditions on rubble shear strength in the IMD laboratory are minimal.

3.5.4 Summary and recommendations

The present study has demonstrated the application of various direct shear methods for the measurement of laboratory ice rubble shear strength *in situ*. The averaged results of $\phi = 41°$ and c = 873 Pa are similar to results reported in the literature. Based on the results of the present experiments, a direct, horizontal shear technique is suitable for determining the *in situ* shear properties of rubble in first year ridge keels. Also, as long as a competent consolidated layer is present, this can be used as a platform for loading the shear plane thus simplifying the testing apparatus. Since trenching around the sides of the ice sample will be a time-consuming operation in the field, the test procedure might be significantly stream-lined by cutting the sides of the ice sample with a slight flare angle. This would eliminate binding of the sample in the hole and enable a single chain saw cut to be used instead of a trench.

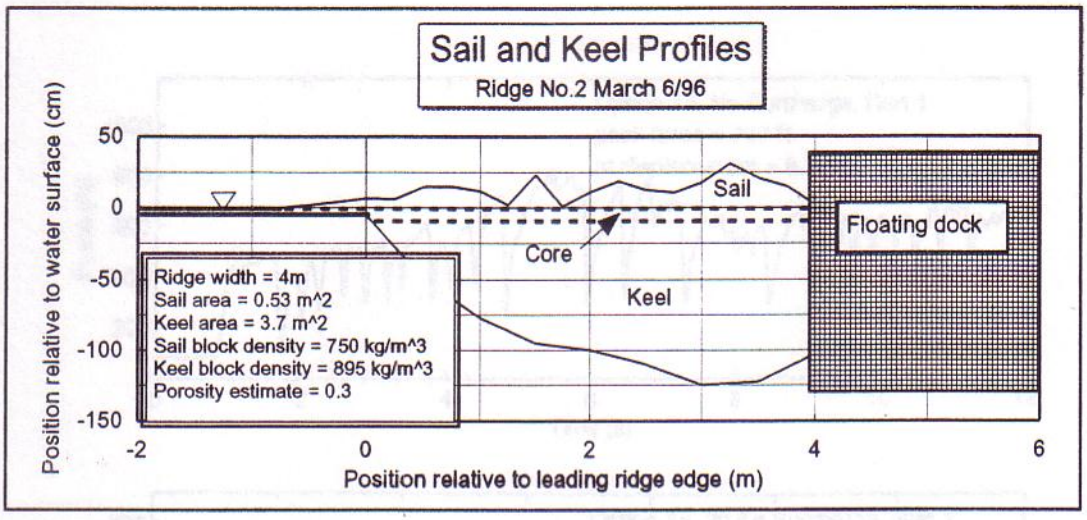

Figure 3.22 Ridge geometry.

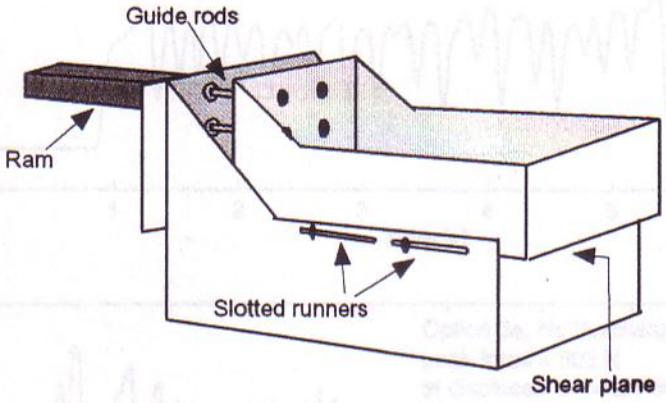

Figure 3.23 Schematic of shear box assembly.

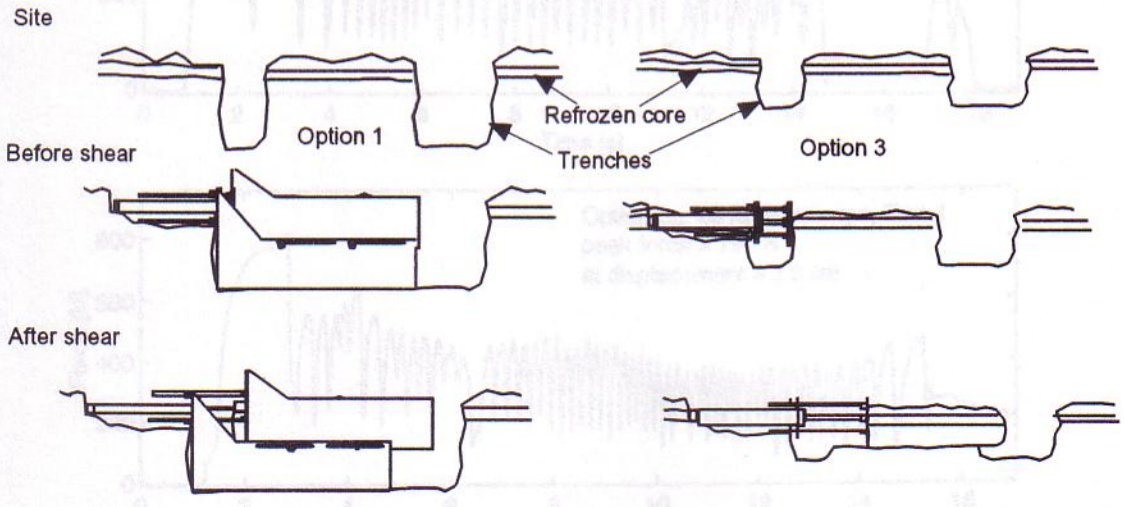

Figure 3.24 Schematic of *in situ* tests, options 1 and 3.

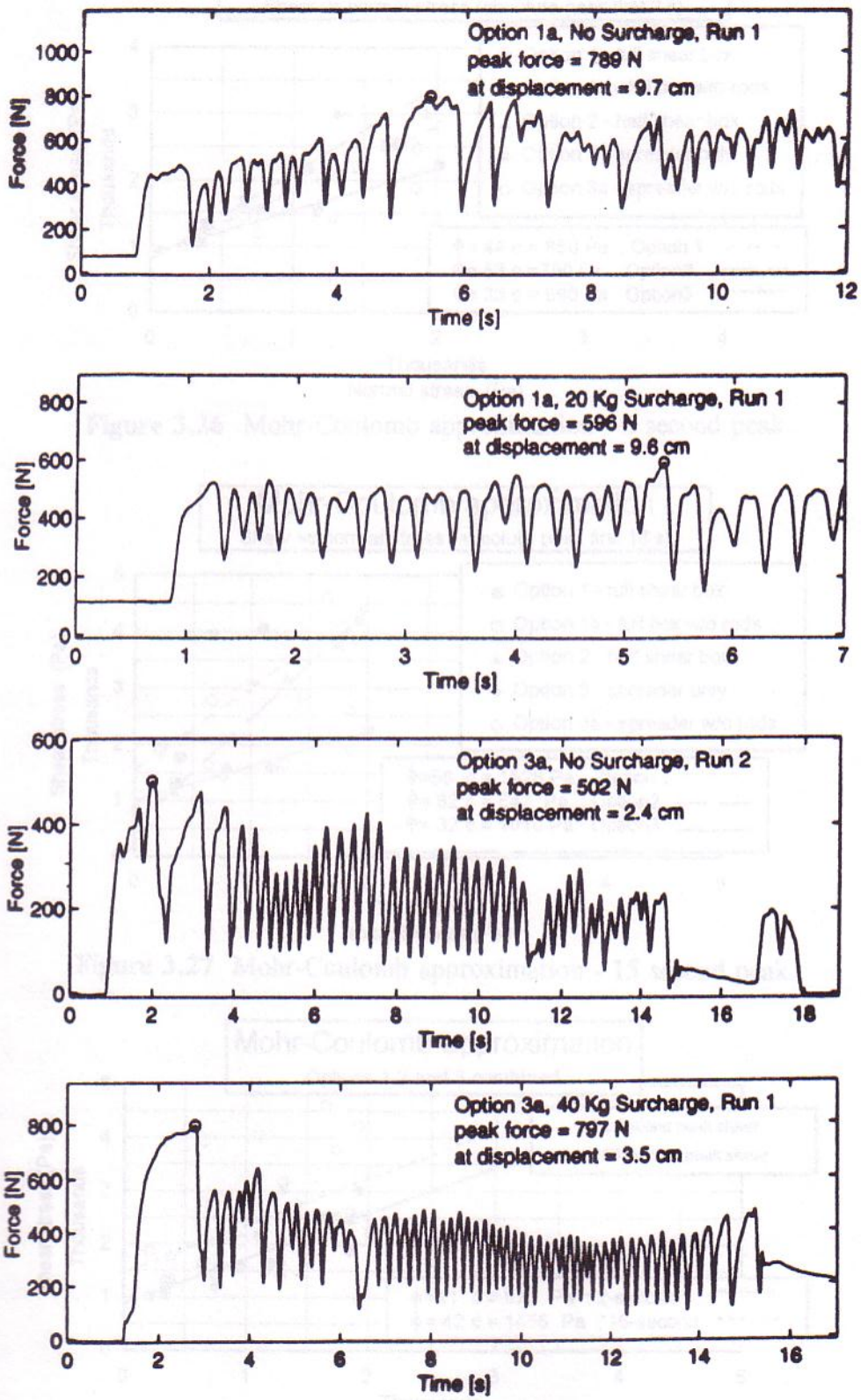

Figure 3.25 Sample force time series.

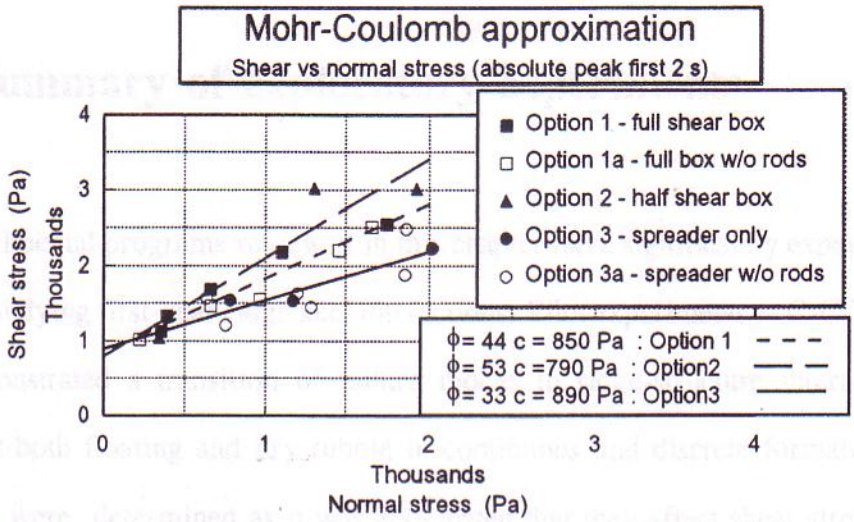

Figure 3.26 Mohr-Coulomb approximation - 2 second peak.

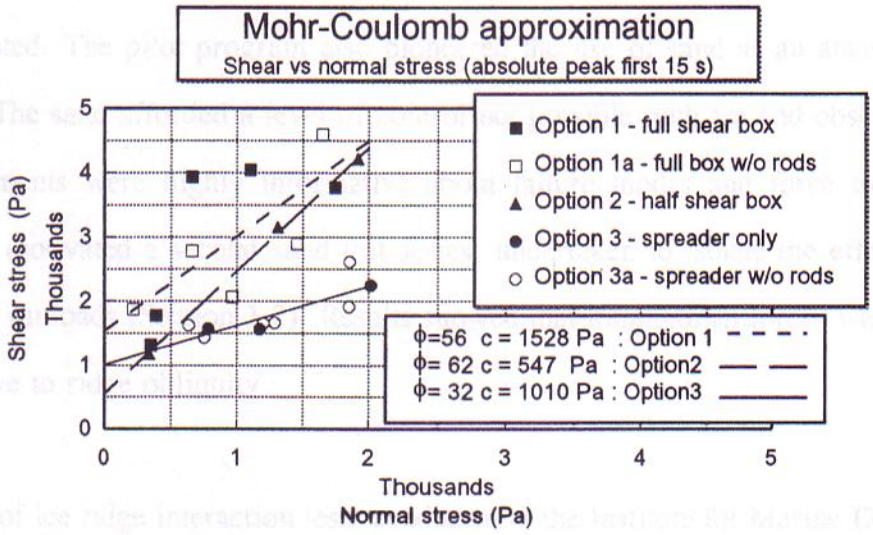

Figure 3.27 Mohr-Coulomb approximation - 15 second peak.

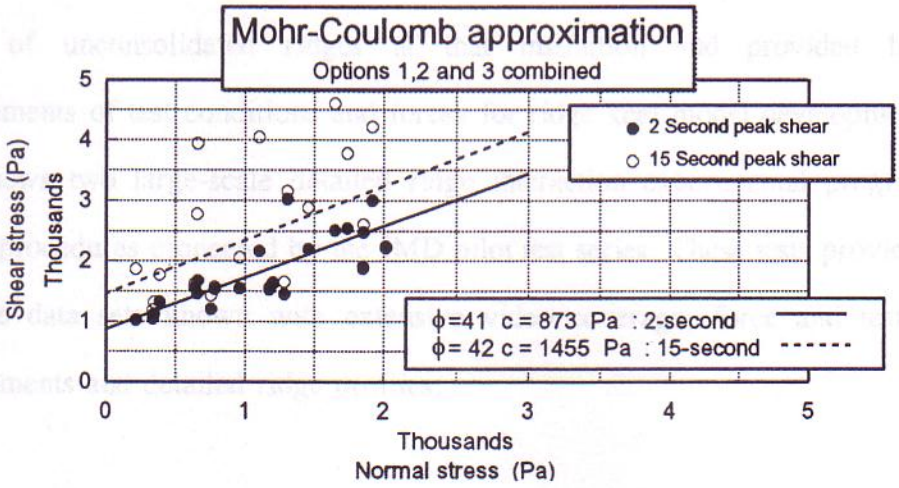

Figure 3.28 Mohr-Coulomb approximation - combined study.

3.6 Summary of exploratory experiments

The experimental programs reviewed in this chapter have significantly expanded the data base for studying first-year ridge keel interactions. Pilot experiments at C-CORE (Section 3.1) demonstrated a transition of failure modes in ridge-structure interactions while looking at both floating and dry rubble in continuous and discrete formations. Rubble properties were determined as it was anticipated that they affect shear strength and the dependency of shear strength on block contact duration and initial temperature was investigated. The pilot program also pioneered the use of sand as an analogue for ice rubble. The sand afforded a level of control not possible with ice and observations and measurements were highly informative about failure modes and force trends. These qualities motivated a second sand test series, undertaken to isolate the effects of ridge obliquity on loads (Section 3.2). Results showed that longitudinal forces were relatively insensitive to ridge obliquity.

A series of ice ridge interaction tests conducted at the Institute for Marine Dynamics are described in Subsections 3.3 and 3.4. The IMD pilot tests in Section 3.3 initiated the testing of unconsolidated ridges at that institution and provided high-quality measurements of test conditions and forces for ridge keel model development. Section 3.4 reviews two large-scale detailed ridge interaction experimental programs which utilized procedures pioneered by the IMD pilot test series. These tests provide the most complete data sets known with extensive video coverage, force and test condition measurements and detailed ridge profiles.

The last experimental program described is one in which a technique for measuring first-year ridge keel shear strength *in situ* was developed. A small-scale model of a proposed apparatus was constructed and tested at IMD providing direction for full-scale tests and adding another set of laboratory ice rubble shear strength data to the literature.

These programs were all directed at diminishing both parametric and force model uncertainties for first-year ridge keel load modelling. In addition to the individual merit of each program, the new data when combined with that from the literature (reviewed in Chapter 2) provides a unique opportunity for the systematic development of an analytical force model. The remainder of this thesis is dedicated to exploiting this opportunity. The first major step described in the next chapter is a regression study. The well-documented and far-reaching data set now assembled permits a broad and meaningful multi-variable regression.